J. Fluid Mech. (1981), *vol.* 111, *pp.* 283–318
Printed in Great Britain

Turbulence in plane channel flows

By M. M. M. EL TELBANY AND A. J. REYNOLDS
Department of Mechanical Engineering, Brunel University,
Uxbridge, Middlesex, England

(Received 10 June 1980)

This paper complements an earlier study of the mean velocities in turbulent flows in a flat channel, one of whose walls can move relative to the other, so that the role of the stress gradient within the wall layers can be varied widely and in a controlled manner.

Measurements of longitudinal, normal and lateral velocity fluctuation intensities (u', v', w') and of shear stresses have been made in essentially fully developed flows established by various combinations of pressure gradient and wall velocity. The channel aspect ratio (breadth/height) has been varied between 12 and 28 and the development ratio (development length/height) between 20 and 45. The introduction of a turbulence-generating grid at the entrance to the duct increases the effective development length.

The study has considered twenty-six flows that are two-dimensional in the mean, which have been established by blowing and relative motion either in the same direction or directly opposed. Empirical descriptions, based on similarity laws incorporating either the wall stress or the local stress, are developed for the turbulence near the walls and in the core. The profiles of u', v' and w' coalesce, to a reasonable approximation, when normalized with appropriate length and velocity scales. Extensive 'plateau' regions are identified, in which the scaled intensities are sensibly constant.

A number of quantities characteristic of the structure of the turbulence are considered, in order to elucidate the effect of the stress gradient on the wall layer, and stages in the erosion of the constant-stress layer are identified.

1. Introduction

The measurements described in this paper were undertaken in conjunction with a study of mean-velocity distributions in plane turbulent channel flows (El Telbany & Reynolds 1980). The objectives of this work are, firstly, the determination of the effect of the stress gradient on the turbulence of fully developed flows between parallel walls and, secondly, the study of the breakdown of the 'constant-stress' layer commonly found in turbulent flow adjacent to a wall.

The flows studied are those in a flat channel (aspect ratio 12 to 28 in these tests) through which air is blown, and one of whose sides consists of a flat belt which can be moved either with the air blown through the channel or in the opposite direction. The experimental situation is shown schematically in figure 1. It is supposed that the motion near the midplane and exit from this channel, that is, in the vicinity of the access ports shown, approximates to fully developed, unidirectional motion.

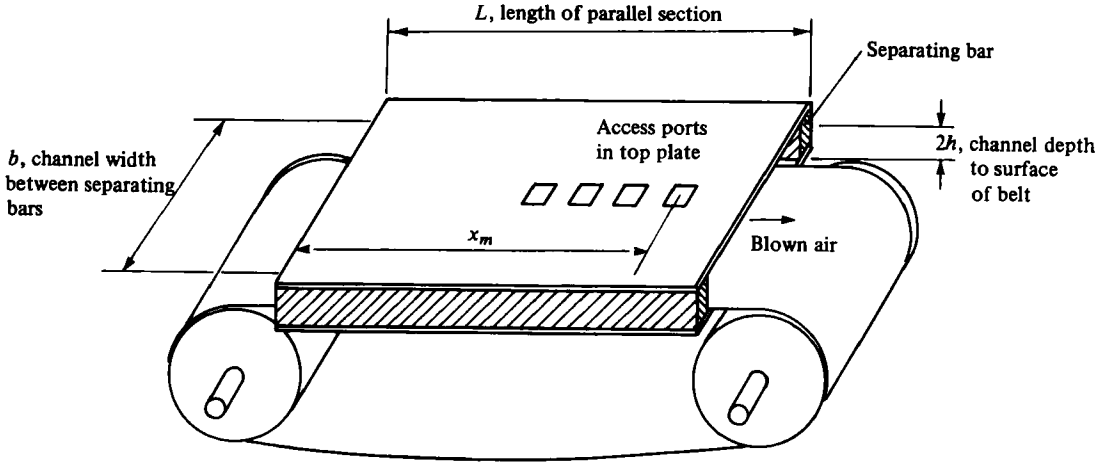

FIGURE 1. Schematic view of test channel showing the belt which provides the moving wall.

An understanding of the effect of the shear-stress gradient on turbulent wall layers requires at the very least a knowledge of the variations of the component intensities throughout such flows. Earlier workers have studied the turbulence structure of two particular flows of the class considered here: pure pressure or plane Poiseuille flow (Laufer 1951; Comte-Bellot 1965; Hussain & Reynolds 1975) and pure shearing or plane Couette flow (Robertson & Johnson 1970). We know of no investigation for more varied combinations of blowing velocity and belt speed, although Hanjalić (1970) examined an asymmetric pressure flow in which differing wall stresses were achieved by roughening one wall.† Mention may also be made of related work on the relaminarization of developing boundary layers by Launder & Stinchcombe (1967), Patel & Head (1968), Badri Narayanan & Ramjee (1969) and Bradshaw (1969).

The present measurements are of general application in providing insight into the role of the shear-stress gradient in a broad class of turbulent wall layers. We consider layers where the shear stress decreases away from the wall, as well as those where the shear stress exceeds that at the wall. However, all of the flows we consider are characterized by the absence of significant deviation of the upstream 'history' of the flow from the local conditions.

2. Details of experiments

2.1. *Apparatus*

The parallel section of the channel shown in figure 1 is 2440 mm long. The main measurements were made in the central plane of the channel at a station $x_m = 1980$ mm from the blowing end. The belt forming the moving floor is 1200 mm wide, some 20 mm less than the channel breadth measured between the separating bars which form the vertical sides. To eliminate possible flapping, the belt is supported below by an aluminium-surfaced plate. Tensioning and central running on the slightly crowned rollers are achieved by screw adjustment of the bearings supporting one of the rollers.

† See also Hanjalić & Launder (1972). Flows in which the planes of maximum velocity and zero shear stress do not coincide have been considered also by Taillard & Mathieu (1967); Spettel, Mathieu & Brison (1972) and Alcaraz, Charney & Mathieu (1975).

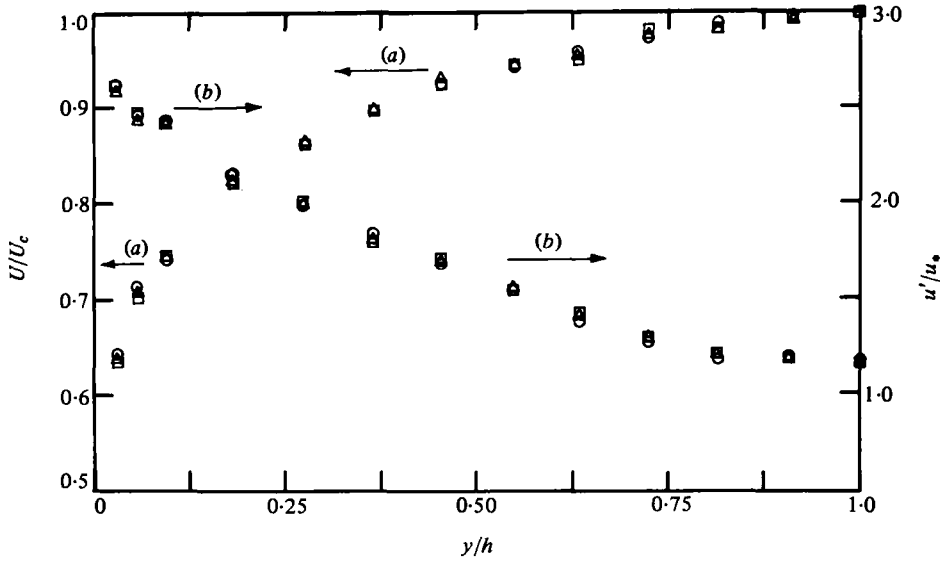

FIGURE 2. Mean-velocity and longitudinal-intensity profiles at three different streamwise locations for pure pressure flow. All the three stations are on the central plane: △, station 1, $x/2h = 30{\cdot}0$ ($x = 1980$ mm); ○, station 2, $x/2h = 25{\cdot}4$ ($x = 1675$ mm); □, station 3, $x/2h = 20{\cdot}8$ ($x = 1370$ mm) (x measured from the blowing end). (*a*) Mean-velocity profiles. (*b*) Longitudinal-intensity profiles.

The plate forming the top of the channel is stiffened to maintain uniformity of channel depth and is clamped to the separating bars, which can be changed to alter the depth. The depths used in our experiments range from $2h = 44$ mm to 101 mm, giving aspect ratios $b/2h = 28$ to 12, and scaled development distances $x_m/2h = 45$ to 20.

The flow into the test channel is supplied by a specially constructed open-circuit wind tunnel, consisting of centrifugal fan, diffuser, filters and contraction. To expedite the development of the flow, turbulent activity is introduced before the air enters the parallel-sided duct, by a coarse mesh of expanded metal located some 150 mm upstream of the parallel section. The mean-velocity profiles of figure 2(*a*), and the longitudinal intensity profiles of figure 2(*b*) (for measuring stations $x = 1370$ mm, 1675 mm and 1980 mm and for pure pressure flow) demonstrate that the turbulent motion is substantially fully developed at the standard measuring station, $x_m = 1980$ mm. Similar measurements made in the absence of the turbulence-inducing mesh displayed significant changes from one station to the next. Moreover, comparisons of longitudinal intensities in Couette flow, measured at $x_m = 1980$ mm with and without the mesh in position, revealed the increase in the intensity to be typically $\Delta(u'/U_c) \simeq 0{\cdot}15\,\%$ or $\Delta u'/u' \simeq 2\,\%$ when the mesh was introduced.

The longitudinal velocity fluctuation was measured using a DISA normal hot-wire probe (type 55P11) in conjunction with a DISA 55M system constant-temperature anemometer, a 55M25 linearizer, a 55D35 r.m.s. voltmeter and a Datron 1045 digital voltmeter. Vertical and lateral velocity fluctuations and the turbulent shear stress were measured with a DISA X-wire probe (type 55P61) in conjunction with two such channels, the r.m.s. voltmeter and the digital voltmeter.

The position of the hot-wire probes within the channel could be controlled within

0·01 mm by a micrometer traversing mechanism. The belt speed was determined by a counter activated by magnetic strips on the belt.

2.2. *Interpretation of hot-wire signals*

The basic theory of operation of the hot-wire anemometer is well covered in the literature; the development which follows leads to results given by Champagne & Schleicher (1967) and Hinze (1975).

To specify the turbulent flow in our rectangular channel, we adopt Cartesian co-ordinates: x in the mean flow direction, y normal to the walls and z in the transverse direction. The velocity components are $\overline{U}+u$, v and w, where the bar denotes time averaging, and u, v and w are the velocity fluctuations in x, y and z directions, respectively. The equations used to determine $\overline{u^2}$, $\overline{v^2}$ and $\overline{uv}$ are:

$$\overline{u^2} = \frac{\overline{e_1^2}}{c^2}, \tag{2.1}$$

$$\overline{v^2} = \frac{\overline{e_2^2}+\overline{e_3^2}-(1+k^2)\,\overline{e_1^2}}{c^2(1-3k^2)}, \tag{2.2}$$

$$\overline{uv} = \frac{\overline{e_2^2}-\overline{e_3^2}}{2c^2(1-k^2)}. \tag{2.3}$$

Analogously, from wires lying in the x, z plane

$$\overline{w^2} = \frac{2\overline{e_4^2}-(1+k^2)\,\overline{e_1^2}}{c^2(1-3k^2)} \tag{2.4}$$

on the assumption of statistical symmetry about the x, y plane, where c is the sensitivity of the linearized equation and k is the yaw sensitivity factor (Webster 1962; Champagne, Sleicher & Wehrmann 1967; Lawn 1969; Kanevce & Oka 1973).

The values of $\overline{e_1^2}$, $\overline{e_2^2}$ and $\overline{e_3^2}$ are obtained with a normal probe in the y, z plane for $\overline{e_1^2}$ and an x-probe in the x, y plane for $\overline{e_2^2}$ and $\overline{e_3^2}$. To obtain $\overline{e_4^2}$ the X-probe is located in the x, z plane. Most of the measurements were repeated several times with different pairs of hot wires to eliminate the systematic error incurred with any one pair.

Acrivlellis (1977) has suggested an alternative way of analysing slant-wire signals. We carried out the calculations using both methods, finding that Acrivlellis's results gave very much lower values for $\overline{v^2}$ and $\overline{w^2}$. In view of the pronounced three-dimensional character of turbulent mixing, these predictions seemed less realistic, and the results presented are those of the more widely used method of analysis (equations (2.1)–(2.4)).

3. Similarity analysis

In seeking to present our measurements in a compact manner, we shall adopt the least controversial analytical framework. Accordingly, we rely in the main on simple dimensional arguments. Perry & Abell (1977) have gone rather further with the predication of the variation of turbulence intensities in fully developed channel flow,

basing their analysis on Townsend's (1961) consideration of mean velocity variation.

The time-mean velocity at a point in fully developed flow of the kind under discussion can be written

$$U/u_* = f(yu_*/\nu, \alpha h/u_*^2, y/h) \tag{3.1}$$

as was shown in El Telbany & Reynolds (1980). Similarly the r.m.s. turbulence fluctuations can be represented:

$$\frac{u'}{u_*}, \frac{v'}{u_*}, \frac{w'}{u_*} = f\left(\frac{yu_*}{\nu}, \frac{\alpha h}{u_*^2}, \frac{y}{h}\right), \tag{3.2}$$

where y is the distance measured from one wall; $u_* = (\tau_w/\rho)^{\frac{1}{2}}$ is the friction velocity based on the shear stress τ_w at the wall from which y is measured; ρ is the density of the fluid; ν is the kinematic viscosity of the fluid; h is half the distance between the parallel walls; and α is gradient of the kinematic shear stress. Note that $|\alpha| = |(\tau_1 - \tau_2)/2\rho h| = |\partial(\tau/\rho)/\partial y|$, where τ_1 and τ_2 are the stresses at the two walls, with the subscript 1 denoting the wall at which the stress is the greater and the subscript 2 the other wall.

Below we develop some specific forms from the general relationship (3.2), and these suggest ways in which the measurements can be presented coherently. Three velocity scales will be considered:

(a) friction velocity based on the shear stress at the adjacent wall, $u_* = (\tau_w/\rho)^{\frac{1}{2}}$,

(b) friction velocity based on the local shear stress, $u_L = (\tau/\rho)^{\frac{1}{2}}$, and

(c) an effective friction velocity† combining the effects of the two walls

$$u_e = (u_{*1}^2 + u_{*2}^2)^{\frac{1}{2}} = [(|\tau_1| + |\tau_2|)/\rho]^{\frac{1}{2}}. \tag{3.3}$$

Evidently the first may be expected to be appropriate immediately adjacent to a wall, the second perhaps over a more extensive wall layer, and the third possibly in the central core of the flow.

A number of length scales can also be distinguished: (a) the viscous scale ν/u_*, a measure of the distance from the wall at which the effects of viscosity *cease* to be significant; (b) the gradient scale $u_*^2/|\alpha|$, a measure of the distance from the wall at which the effects of the stress gradient *begin* to be significant; (c) the channel half-width h; and (d) the distance y_m from the wall to the point of maximum velocity. The applicability of these scales may be expected to parallel that of the three friction velocities. Note, however, that scale (d) is defined only for Poiseuille-type flows ($\gamma = \tau_2/\tau_1 < 0$), while ($b$) is not defined for pure Couette flow ($\gamma = 1$, $\alpha = 0$).

In characterizing the various flows and wall layers, we shall use several dimensionless parameters.

(a) $\gamma = \tau_2/\tau_1$ is the wall-stress ratio referred to above.

(b) $\lambda = |\alpha|h/u_*^2 = h/(u_*^2/|\alpha|)$ is a measure of the significance of the stress gradient relative to the stress at one wall. (We can also distinguish $\lambda_1 = \alpha_1 h/u_{*1}^2$ and $\lambda_2 = \alpha_2 h/u_{*2}^2$.) Alternatively, λ can be interpreted as the ratio of the length scales (c) and (b) introduced above.

(c) $\mu = u_*^3/(|\alpha|\nu) = (u_*^2/|\alpha|)/(\nu/u_*)$ is a ratio of the length scales (b) and (a) introduced above. (We can also distinguish $\mu_1 = u_{*1}^3/(\alpha_1\nu)$ and $\mu_2 = u_{*2}^3/(\alpha_2\nu)$.)

† This particular combination has been selected as representing the total turbulence energy of the flow, the sum of two quantities which characterize the energy introduced at the two walls.

This parameter is an indicator of the possible interaction between the effects of stress gradient and viscosity; the two can be influential in the same part of the flow only if $u_*^2/|\alpha|$ is small enough and ν/u_* large enough, together giving a sufficiently small value of μ.

3.1. *Wall-stress scaling*

If the influence of the stress gradient does not penetrate too close to a smooth wall, there will exist near it a region where

$$u'/u_* = f(yu_*/\nu) = f(y^+) \quad \text{only}, \tag{3.4}$$

with similar expressions for the other components.

Simple momentum and continuity arguments applicable immediately adjacent to the wall indicate that

$$\left.\begin{aligned} u'/u_* &= A_1 yu_*/\nu \quad \text{or} \quad u'/u_* y^+ = A_1, \\ v'/u_* &= A_2(yu_*/\nu)^2 \quad \text{or} \quad v'/u_* y^{+2} = A_2, \\ w'/u_* &= A_3 yu_*/\nu \quad \text{or} \quad w'/u_* y^+ = A_3, \end{aligned}\right\} \tag{3.5}$$

where A_1, A_2 and A_3 are constants.

Moreover, in the viscosity-independent region farther from the wall, but not so distant that the other wall influences the flow (through the parameters h and α), equations (3.2) reduce to

$$u'/u_* = B_1, \quad v'/u_* = B_2, \quad w'/u_* = B_3 \tag{3.6}$$

with B_1, B_2 and B_3 constants. We shall refer to the part of the flow where these results may apply as the 'plateau' region.

From the experimental results to be presented later it will be possible to estimate these constants, and to discover the limits to the applicability of these simple formulae. Moreover, we shall find that there exist regions for which it may be useful to generalize equations (3.5) to

$$\left.\begin{aligned} u'/u_* &= C_1 - D_1 y|\alpha|/u_*^2, \\ v'/u_* &= C_2 - D_2 y|\alpha|/u_*^2, \\ w'/u_* &= C_3 - D_3 y|\alpha|/u_*^2, \end{aligned}\right\} \tag{3.7}$$

and to

$$\left.\begin{aligned} u'/u_{*1} &= E_1 - F_1 y/y_{m1}, \\ v'/u_{*1} &= E_2 - F_2 y/y_{m1}, \\ w'/u_{*1} &= E_3 - F_3 y/y_{m1}. \end{aligned}\right\} \tag{3.8}$$

3.2. *Local-stress scaling*

Corresponding to each of the results developed above, we can write down an expression involving the local stress in place of the wall stress, and it is plausible to suppose that these results (which are indistinguishable from those above when $|\alpha|y/u_*^2 = \lambda y/h \ll 1$) will cause the data to coalesce over a wider region of the flow.

Leaving the length scale ν/u_* unaltered, we have:

$$u'/u_L y^+ = A_4, \quad v'/u_L y^{+2} = A_5, \quad w'/u_L y^+ = A_6 \tag{3.9}$$

		Overall characteristics						Parameters for high-stress wall				Parameters for low-stress wall					
Case	Symbol	$2h$ (mm)	U_b ($m\,s^{-1}$)	U_m ($m\,s^{-1}$)	U_a ($m\,s^{-1}$)	$\frac{Re_a}{1000}$	$\frac{Re_b}{1000}$	u_{*1} ($m\,s^{-1}$)	α_1	λ_1	μ_1	u_{*2} ($m\,s^{-1}$)	α_2	λ_2	μ_2	γ	Wall in motion
1	▼	66	12·84	12·84	6·42	28·50	57·01	0·282	0	0	∞	0·282	0	0	∞	1·000	2
2	○	66	12·84	12·84	7·28	32·33	57·01	0·328	−0·808	−0·248	−2940	0·233	0·808	0·491	1050	0·504	2
3	●	66	12·84	12·84	8·06	35·80	57·01	0·362	−1·486	−0·375	−2140	0·1809	1·486	1·499	268	0·250	2
4	△	66	12·84	12·84	8·14	36·14	57·01	0·357	−1·510	−0·391	−2030	0·1667	1·510	1·795	206	0·217	1
5	▽	66	12·84	12·84	8·81	39·11	57·01	0·383	−1·960	−0·442	−1920	0·1305	1·960	3·809	76	0·116	1
6	◒	66	8·59	8·59	6·71	29·79	38·14	0·313	−1·430	−0·481	−1450	0·0615	1·430	12·45	11·0	0·0386	1
7	◓	101	17·08	17·08	14·55	98·80	16·05	0·600	−3·548	−0·497	−4100	0·0400	3·548	112·0	1·21	0·0044	1
8	◪	101	12·84	12·84	11·38	77·30	87·24	0·485	−2·323	−0·498	−3300	0·0229	2·323	223·7	0·348	0·00223	1
9	◇	101	8·59	8·59	7·79	52·94	58·36	0·350	−1·212	−0·499	−2380	0·0084	1·212	867·4	0·033	0·00057	1
10	◆	66	12·84	13·25	12·40	55·07	57·01	0·564	−4·830	−0·501	−2500	0·0300	−4·83	−177·2	−0·376	−0·0028	2
11	□	66	12·84	16·33	15·10	67·05	57·01	0·679	−7·500	−0·537	−2800	0·1860	−7·50	−7·16	−57·6	−0·075	2
12	■	66	12·84	21·57	20·11	89·28	57·01	0·880	−14·30	−0·611	−3200	0·4142	−14·3	−2·76	−334	−0·2215	1
13	*	66	12·84	24·01	22·40	99·48	57·01	0·978	−18·50	−0·640	−3390	0·518	−18·5	−2·28	−504	−0·2805	1
14	×	66	8·59	23·62	21·90	97·25	38·14	0·961	−20·80	−0·742	−2870	0·670	−20·8	−1·529	−972	−0·485	1
15	▲	66	—	16·00	14·55	64·60	—	0·659	−13·14	−1·000	−1460	0·659	−13·1	−1·000	−1460	−1·000	—
16		44	12·84	12·84	6·42	19·00	38·00	0·293	0	0	∞	0·293	0	0	∞	1·000	2
17		44	17·08	17·08	8·54	25·28	50·56	0·378	0	0	∞	0·378	0	0	∞	1·000	2
18		66	17·08	17·08	8·54	37·92	75·83	0·363	0	0	∞	0·363	0	0	∞	1·000	2
19		66	12·84	12·84	6·12	27·17	57·01	0·303	−0·314	−0·113	−5980	0·267	0·314	0·145	4080	0·775	2
20		66	12·84	12·84	3·31	14·70	57·01	0·431	−2·640	−0·468	−2050	0·1089	2·64	7·38	32·7	0·0635	2
21		66	12·84	12·84	3·17	14·07	57·01	0·435	−2·70	−0·471	−2050	0·1035	2·70	8·33	27·6	0·0566	1
22		66	12·84	18·27	16·89	75·02	57·01	0·740	−9·40	−0·566	−2900	0·269	−9·40	−4·28	−140	−0·132	1
23		66	8·59	13·81	12·87	57·13	38·14	0·600	−6·43	−0·591	−2250	0·256	−6·43	−3·25	−175	−0·1816	2
24		66	8·59	15·05	14·02	62·24	38·14	0·645	−7·722	−0·613	−2340	0·306	−7·72	−2·72	−250	−0·225	2
25		44	—	25·80	23·52	69·62	—	1·040	−49·16	−1·000	−1540	1·040	−49·2	−1·000	−1540	−1·000	—
26		66	—	12·60	11·42	50·70	—	0·514	−8·00	−1·000	−1140	0·514	−8·00	−1·000	−1140	−1·000	—

TABLE 1. Details of tests.

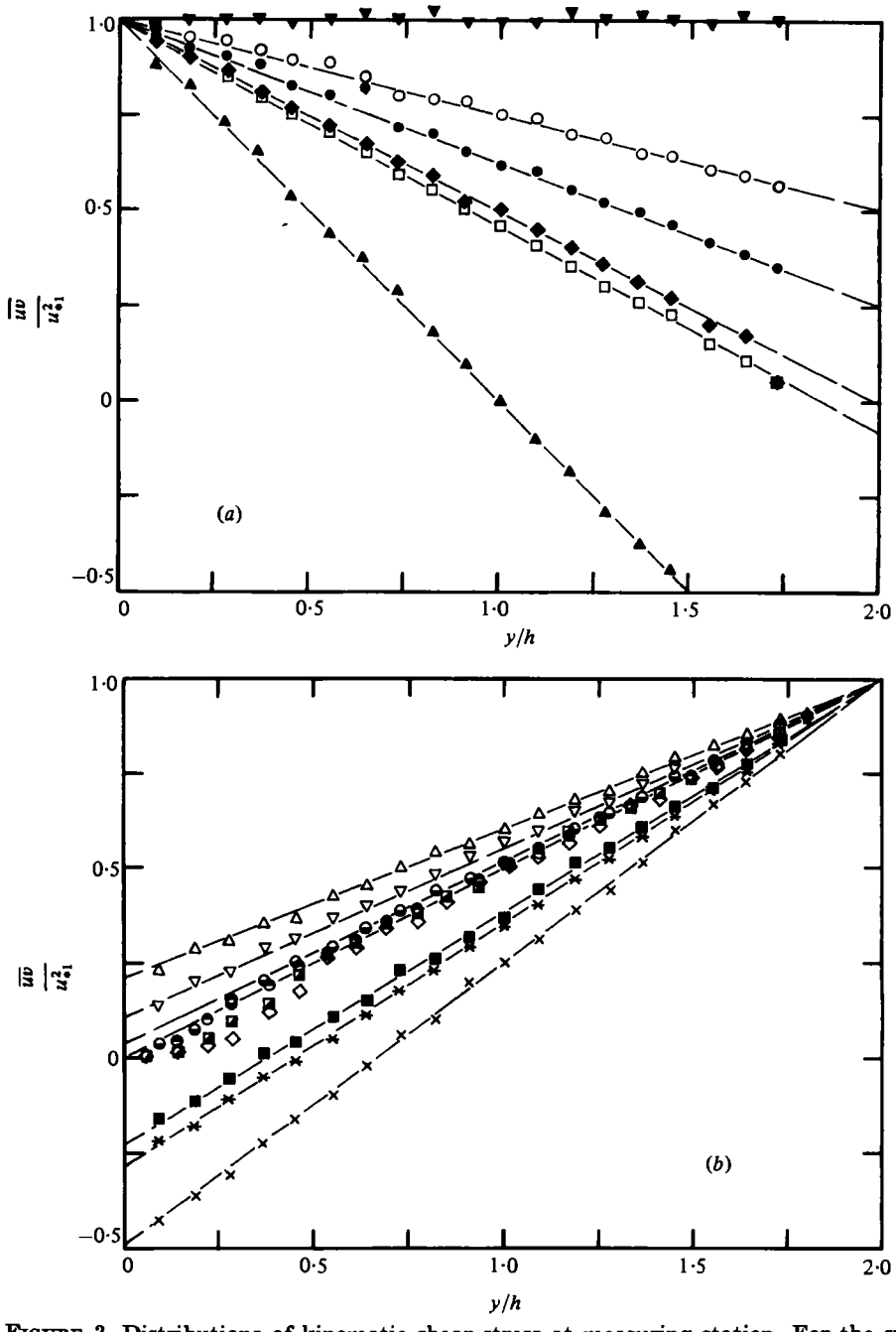

FIGURE 3. Distributions of kinematic shear stress at measuring station. For the symbols, see table 1. (*a*) y measured from the high-stress wall. (*b*) y measured from the low-stress wall.

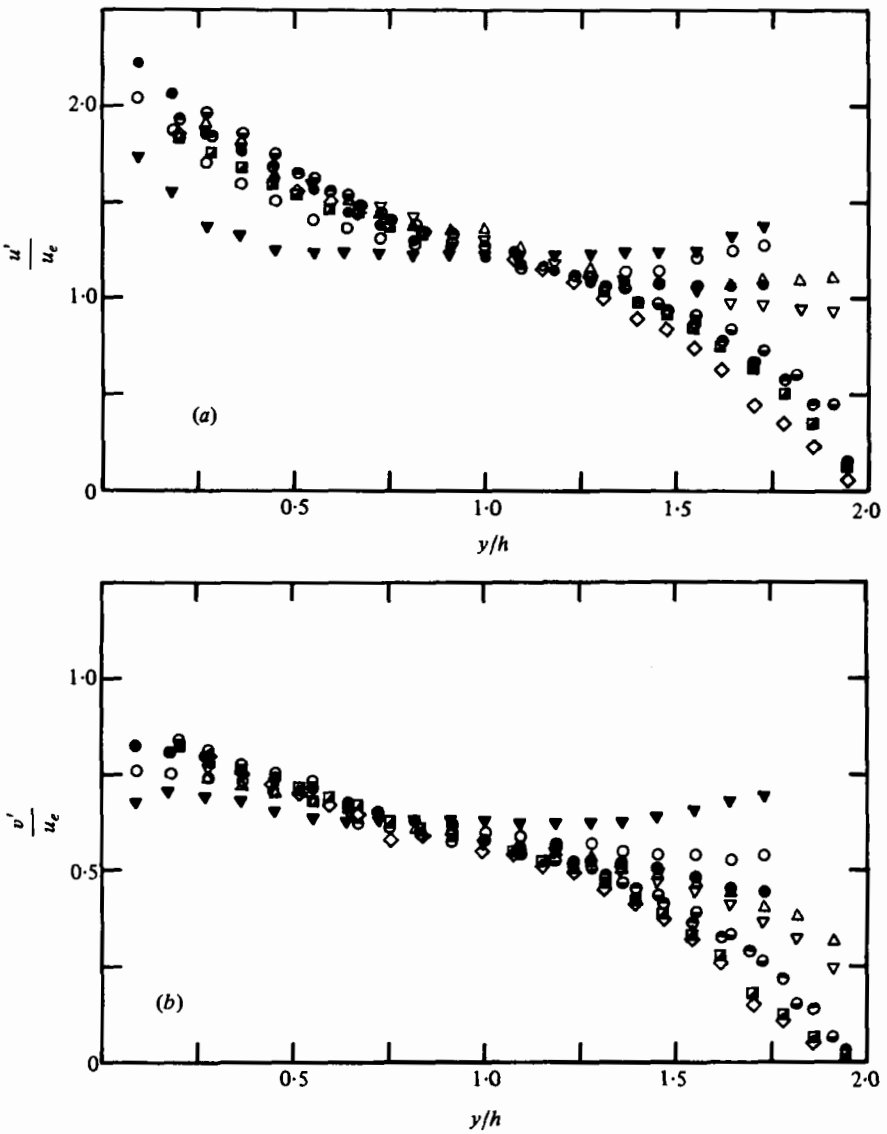

FIGURE 4. Turbulence intensities for Couette-type flows normalized with effective friction velocity (y measured from high-stress wall). For the symbols, see table 1. (*a*) Longitudinal velocity fluctuation. (*b*) Normal velocity fluctuation. (*c*) Lateral velocity fluctuation.

close to the wall, and

$$u'/u_L = B_4, \quad v'/u_L = B_5, \quad w'/u_L = B_6 \tag{3.10}$$

for the viscosity-independent region. These results may define a more extensive 'plateau' region.

We shall also consider the forms

$$u'/u_L = C_4 - D_4 y|\alpha|/u_*^2, \quad v'/u_L = C_5 - D_5 y|\alpha|/u_*^2, \quad w'/u_L = C_6 - D_6 y|\alpha|/u_*^2, \tag{3.11}$$

and

$$u'/u_L = E_4 - F_4 y/h, \quad v'/u_L = E_5 - F_5 y/h, \quad w'/u_L = E_6 - F_6 y/h. \tag{3.12}$$

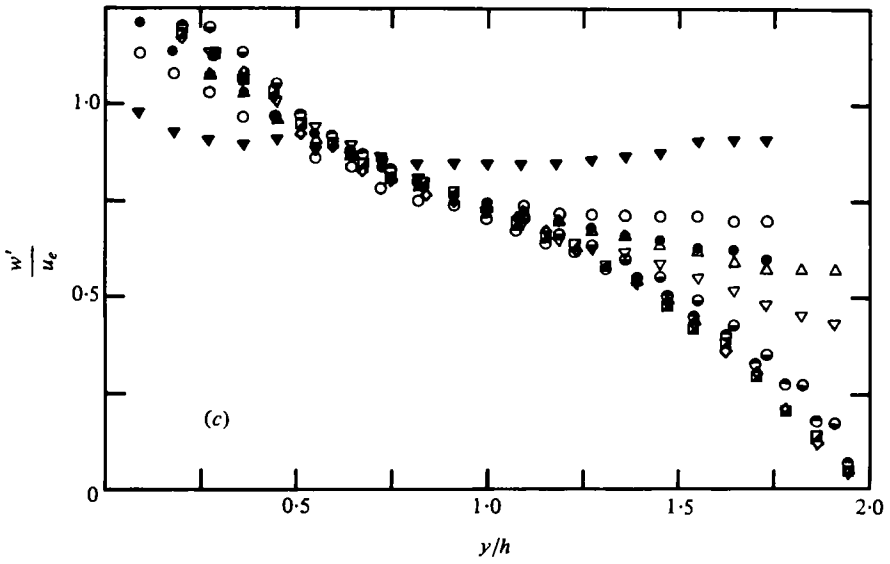

FIGURE 4(c). For legend see p. 291.

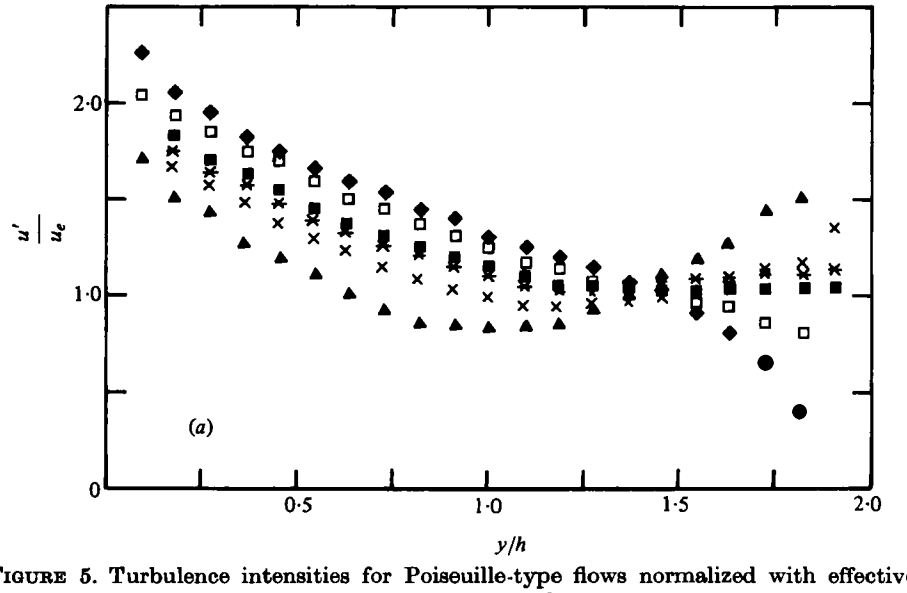

FIGURE 5. Turbulence intensities for Poiseuille-type flows normalized with effective friction velocity (y measured from high-stress wall). For the symbols, see table 1. (*a*) Longitudinal velocity fluctuation. (*b*) Normal velocity fluctuation. (*c*) Lateral velocity fluctuation.

3.3. *Effective-stress scaling*

The most obvious presentation using this scale is

$$u'/u_e, \quad v'/u_e, \quad w'/u_e = f(y/h). \tag{3.13}$$

It is possible, however, that one of the many alternative formulations may be more successful in collapsing the data in the core region between the wall layers.

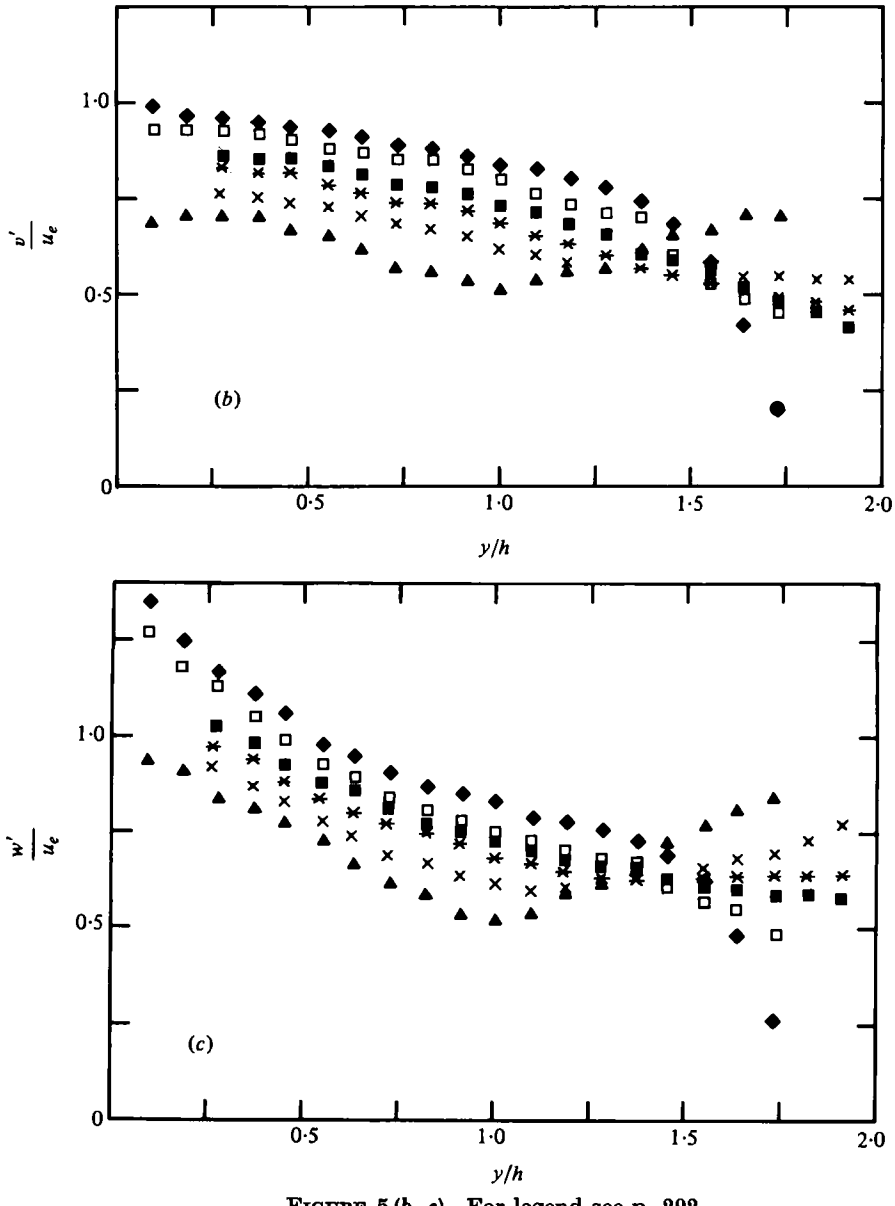

FIGURE 5 (*b*, *c*). For legend see p. 292.

4. Analysis of results

4.1. *Basic results*

Table 1 details the tests carried out. In this table U_b is the velocity of the moving belt, U_a is the average velocity, U_m is the maximum velocity, $Re_a = 2hU_a/\nu$ and $Re_b = 2hU_b/\nu$ are Reynolds numbers. The first group (cases 1–9) are Couette-type flows ($\gamma > 0$); the second group (cases 10–15) are Poiseuille-type flows ($\gamma < 0$). For the remaining flows (cases 16–26) the same measurements were made, but they reproduce the features illustrated by the other cases and will not be described so completely.

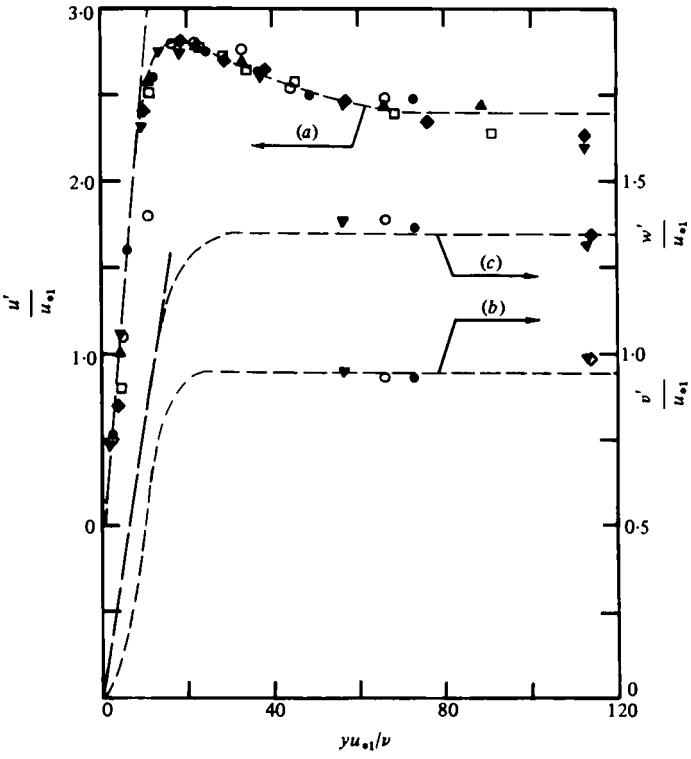

FIGURE 6. Variations of component intensities adjacent to high-stress walls normalized with wall-friction velocity. For the symbols, see table 1. (*a*) Longitudinal velocity fluctuation. *b*) Normal velocity fluctuation. (*c*) Lateral velocity fluctuation.

All but four of these flows were generated by running the belt in the direction of the blown flow of air. For the cases of counter-motion (12–14, 22) the region of reversed flow moving into the belt was very thin, extending at most to $y/2h = 0{\cdot}05$. Hence a close approximation to full development can still be achieved at $x_m = 1980$ mm, despite the small amount of air drawn into the channel from the nominal exhaust section at $x = 2440$ mm.

Figure 3 shows the variations of turbulent shear stress in the fifteen flows selected for study. Wall stresses were found by extrapolating the linear portions to the walls. The probe can be brought close to the fixed wall, but not as near to the moving wall, since any local protuberance on the belt may damage the instrument. Hence one of the two wall layers within each flow can be examined in more detail than can the other. The linearity of the turbulent shear stress is seen to break down near the low-stress wall for cases 6, 7, 8, 9 and 10 because the viscosity-influenced region occupies a significant fraction of the channel when the parameter $\mu < 50$ and $|\gamma| < 0{\cdot}04$.

The turbulence intensities for the Couette-type flows plotted in figure 4 have been scaled using the 'effective' friction velocity of equation (3.3), which is conceived to represent the turbulent activity in the core region, contributed to by the wall layers on either side. Figure 5 gives the intensities for the Poiseuille-type flows, also scaled using the effective friction velocity. The scaling adopted does not bring about a coalescence of the velocity-fluctuation measurements, save in a crude way in an

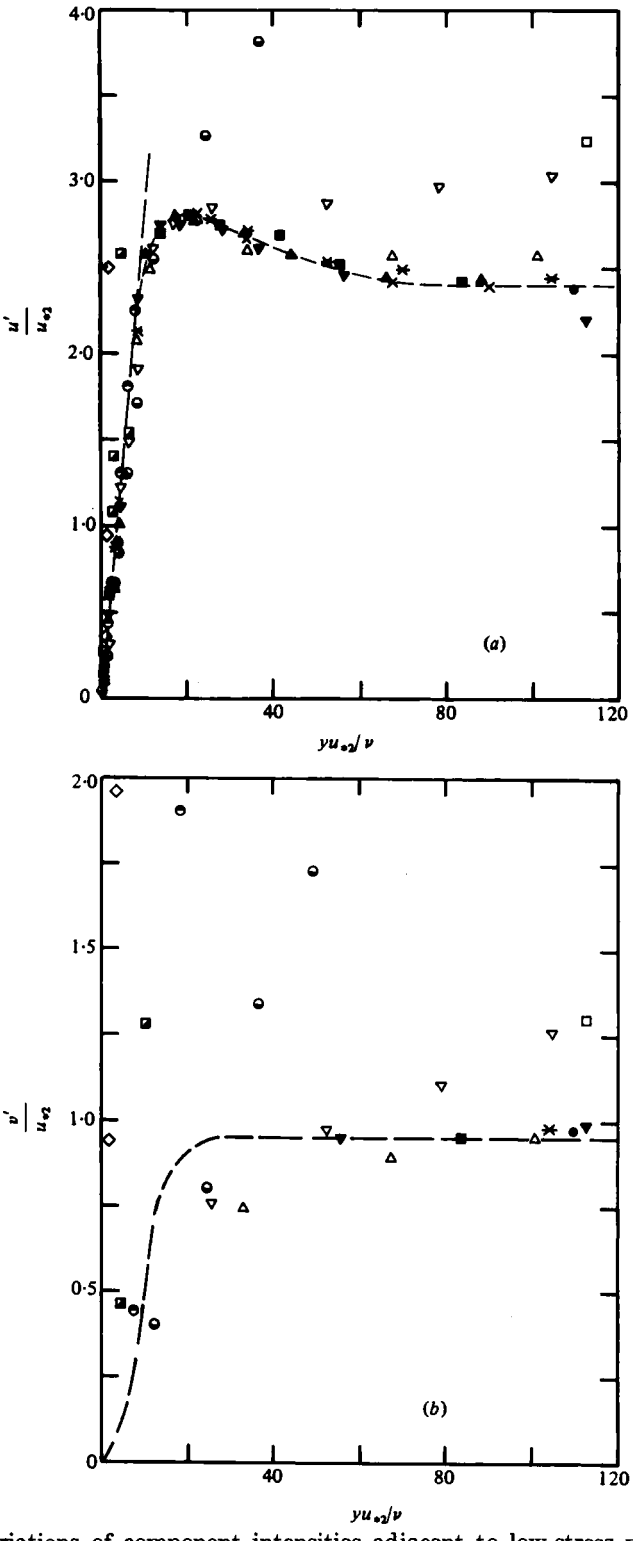

FIGURE 7. Variations of component intensities adjacent to low-stress walls normalized with wall-friction velocity. For the symbols, see table 1. (*a*) Longitudinal velocity fluctuation. (*b*) Normal velocity fluctuation. (*c*) Lateral velocity fluctuation.

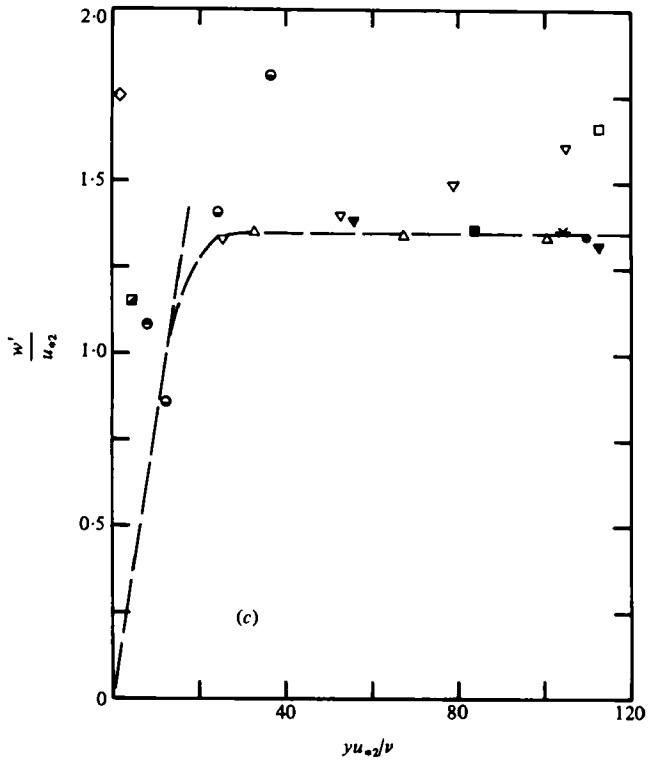

FIGURE 7 (c). For legend see p. 295.

ill-defined central region. Alternative presentations of these results are introduced below.

4.2. *Wall-stress scaling*

Figure 6 shows the variations of the component intensities adjacent to the high-stress walls, plotted according to the wall-stress scaling of equations (3.5), (3.6). The axial intensity u' is the largest over the entire region; its peak value ($u'/u_* \simeq 2{\cdot}8$) is attained near the wall, at $y^+ \simeq 18$. Since the viscous layers are here very thin, the X-probe measurements of v' and w' do not extend into the region of rapid variation near the wall; nevertheless, the 'plateau' values of equations (3.6) are clearly defined.

Figures 7 and 8 give the turbulence intensity distributions adjacent to low-stress walls. For cases with $\mu < 200$ (see table 1) the intensities are significantly greater than those for $\mu > 200$ in the region $y^+ > 40$. However, for cases with $\mu < 10$ the intensities exceed those for $\mu > 10$ in the region $y^+ < 15$, and even closer to the wall for the lowest values of μ.

Table 2 gives the constants of equations (3.5), (3.6) derived from figure 7; note that the same values are indicated by figure 6. It will be noted that the 'plateau' given by wall-stress scaling extends over the range $40 < y^+ < 100$ unless the stress gradient is large ($\mu < 200$). Comparisons of these values with those derived from other measurements are given in table 3; there is fair agreement between our results and those of other investigators. It should be noted, however, that the values characterizing v' and w' in the viscous region are usually – as are ours – estimates based on modest experimental evidence.

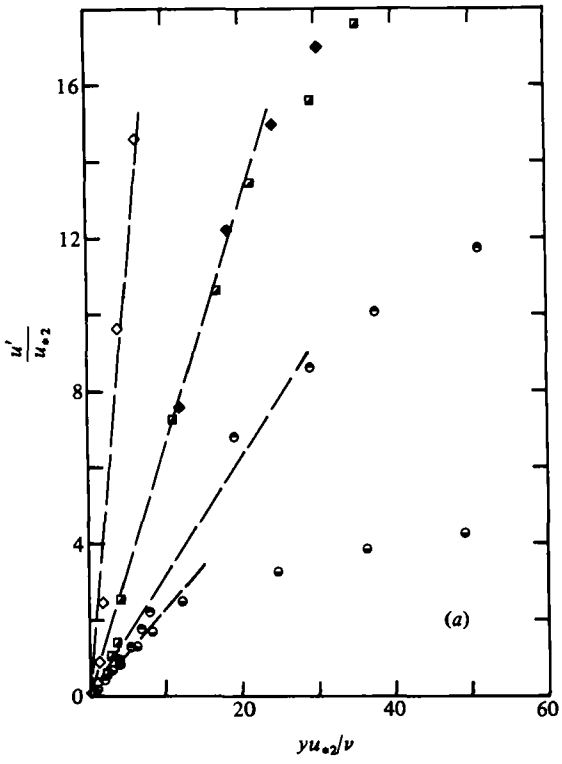

FIGURE 8. Variations of component intensities adjacent to low-stress walls normalized with wall-friction velocity. For the symbols, see table 1. (*a*) Longitudinal velocity fluctuation. (*b*) Normal velocity fluctuation. (*c*) Lateral velocity fluctuation.

4.3. *Local-stress scaling*

In figure 9 the variations of component intensities near the low-stress wall in Couette-type flows are presented in terms of the parameters of equations (3.9), (3.10); table 4 gives constants and limits derived from this figure. Again a clear 'plateau' emerges, but now with a quite different range of applicability:

(1) $y^+ > 50$ for layers with $0{\cdot}1 < \mu < 10$, that is, where the influence of the stress gradient is relatively large;

(2) $y^+ > 165$ for layers with $\mu > 200$, that is, where the stress variation is less significant.

We shall see later that the outer boundary of these plateau regions is given approximately by $y/h = 1{\cdot}35$, that is, by the commencement of the wall layer on the opposite, high-stress wall of the channel.

Figure 10 shows the intensity distributions for the high-stress walls in Couette-type flows, using the scaling of equations (3.11). Case 1, for which $\alpha = 0$, cannot be included, but results for the low-stress wall of case 2 are given. In figure 11 the variations of component intensities for the high-stress walls in Poiseuille-type flows are presented in terms of the parameters of equations (3.11). As in figure 9, local-stress scaling is found to generate a 'plateau' in the core of the flow, but not (for these high-stress layers) near the wall. Individual intensity variations near the wall are approximately linear, but the length scale $|\alpha|/u_*^2$ does not prove to be very effective

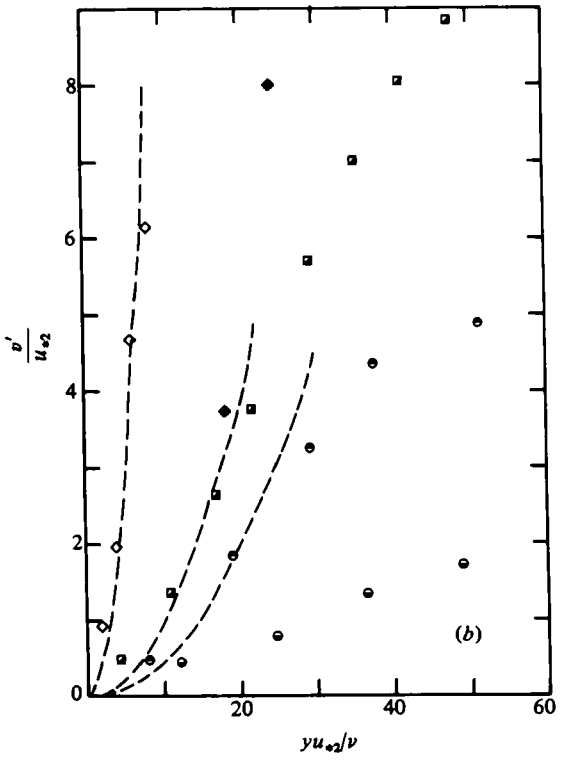

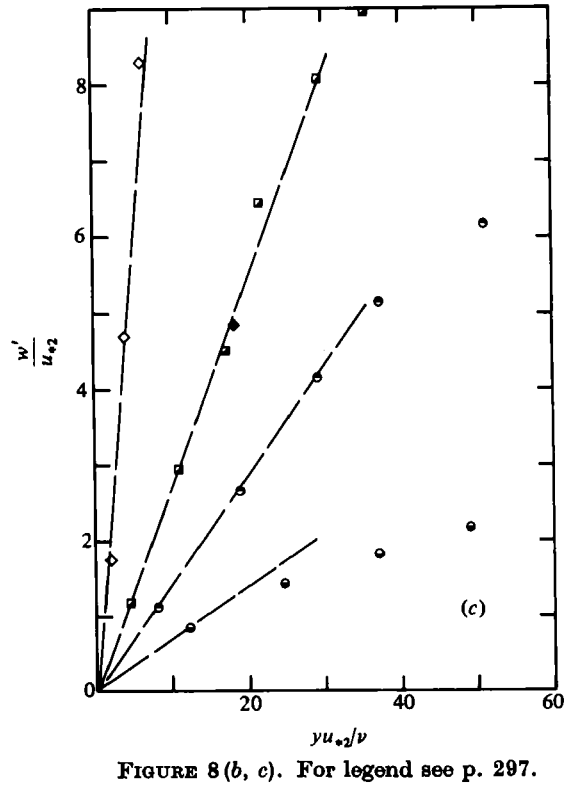

FIGURE 8 (*b*, *c*). For legend see p. 297.

Flows	y^+	Region	μ	u'/u_*	v'/u_*	w'/u_*
Cases 7–10	<15	Viscous	<10	$A_1 y^+$ $A_1 = 0{\cdot}28$ to $2{\cdot}0$	$A_2 y^{+2}$ $A_2 = 0{\cdot}005$ to $0{\cdot}125$	$A_3 y^+$ $A_3 = 0{\cdot}08$ to $1{\cdot}05$
All others	<15	Viscous	>10	$A_1 y^+$ $A_1 = 0{\cdot}28$	$A_2 y^{+2}$ $A_2 = 0{\cdot}005$	$A_3 y^+$ $A_3 = 0{\cdot}08$
All	>40 <100	Plateau	>200	$B_1 = 2{\cdot}4$	$B_2 = 0{\cdot}95$	$B_3 = 1{\cdot}35$
Poiseuille type	—	Core, high-stress side	All	$2{\cdot}12$ $-1{\cdot}11 y/y_{m1}$	$1{\cdot}05$ $-0{\cdot}32 y/y_{m1}$	$1{\cdot}22$ $-0{\cdot}56 y/y_{m1}$

TABLE 2. Similarity results for wall-stress scaling. The higher values in the ranges for A_1, A_2, A_3 represent case 9, the lower values case 6.

in bringing together the data for the several flows. Note also that Poiseuille flow itself is unrepresentative of the broader class of flows for which $0 > \gamma > -1$.

Figure 12 shows the intensity distributions for Couette-type flows plotted according to the local-stress scaling of equations (3.12), where h is the length scale. This presentation is no more effective in collapsing the several sets of near-wall data than was the gradient length scale used in figure 10. Seemingly, the effects of the core flow (represented by h) and of the stress gradient (represented by $|\alpha|/u_*^2$) are of comparable importance in this region, and neither scale alone can define adequate similarity laws for the turbulence.

Approximate formulae patterned on equations (3.11), (3.12) can be developed for this region, for example,

$$\left.\begin{aligned} u'/u_L &= 2{\cdot}3 - 0{\cdot}82y/h = 2{\cdot}6 - 3{\cdot}4y|\alpha|/u_*^2, \\ v'/u_L &= 1{\cdot}0 - 0{\cdot}31y/h = 0{\cdot}98 - 0{\cdot}75y|\alpha|/u_*^2, \\ w'/u_L &= 1{\cdot}4 - 0{\cdot}55y/h = 1{\cdot}45 - 1{\cdot}68y|\alpha|/u_*^2, \end{aligned}\right\} \tag{4.1}$$

valid for a range of Couette flows with $\mu > 200$. However, these results are neither accurate enough nor of sufficiently general application to be worth listing in full.

Referring back to figure 6, we note that wall-stress scaling proved successful in collapsing much of the data for high-stress walls, for which local-stress scaling has now been seen to be ineffective. Summing up, the following simple 'plateau' models for the intensities have been established:

(*a*) with wall-stress scaling, in the region $40 < y^+ < 100$ for any layer with $\mu > 200$;

(*b*) with local-stress scaling, in the region $y/h < 1{\cdot}35$ for Couette-type flows, with the inner boundary given by $y^+ = 165$ for $\mu_2 > 200$, by $y^+ > 50$ for $10 > \mu_2 > 0{\cdot}1$, and by $y^+ = 20$ for $\mu_2 < 0{\cdot}1$. (Here y is measured from the low-stress wall.)

4.4. *Core region: Couette-type flows*

The structure of the turbulence in the core region of Poiseuille-type flows must be expected to be significantly different from that in Couette-type flows, since conditions at the boundaries of the core are so dissimilar.

For Couette-type flows our study of the 'plateau' region extending outwards from the low-stress wall has led to a simple characterization of the turbulence in the central

	Present Channel, $-1 \leqslant \gamma \leqslant 1$	Comte-Bellot (1965) Channel, $\gamma = -1$	Robertson & Johnson (1970) Channel, $\gamma = 1$	Hussain & Reynolds (1975) Channel	Laufer (1954) Pipe	Morrison & Kronauer (1969) Pipe	Klebanoff (1955) Boundary layer	Hatziavramidis & Hanratty (1979) Theoretical
$\frac{u'}{u_* y^+}$	0·28	0·25–0·3	0·31	0·30	0·30	0·30	0·31	0·41
$\frac{u'}{u_*}$	2·4	2·35–2·45	—	2·1	2·1	2·2	—	—
Peak values: $\frac{u'}{u_*}$ (y^+)	2·8 (18)	2·84 (18) –2·8 (16)	2·9 (16)	2·4 (14)	2·65 (17)	3·0 (16)	3·05 (19)	3·25 (10)
$\frac{v'}{u_* y^{+2}}$	0·005	—	—	—	0·007	—	—	0·003
$\frac{v'}{u_*}$	0·95	—	—	—	0·90	—	0·905	—
$\frac{w'}{u_* y^+}$	0·08	—	—	—	0·08	—	0·07	0·10
$\frac{w'}{u_*}$	1·35	—	—	—	1·3–1·7	—	1·73	1·30

TABLE 3. Comparisons of wall-stress scaling data.

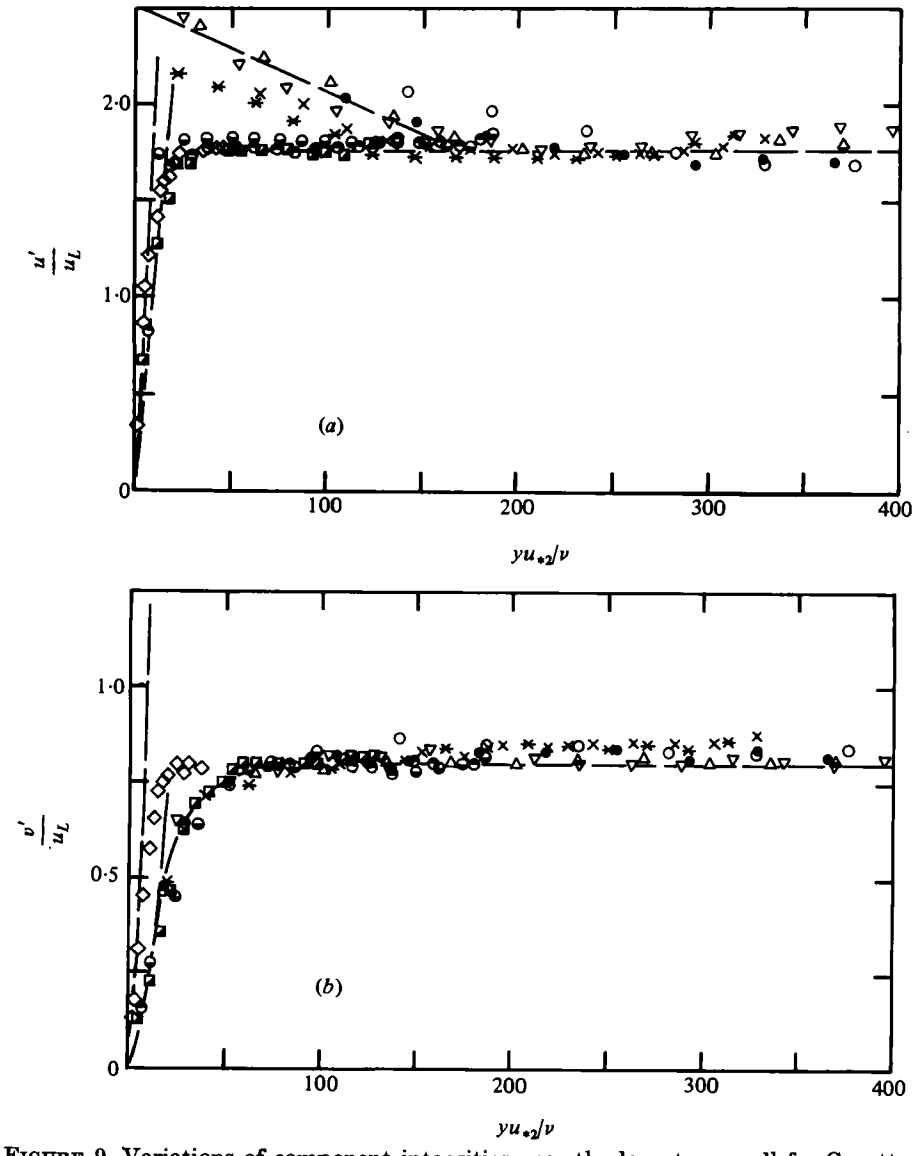

FIGURE 9. Variations of component intensities near the low-stress wall for Couette-type flows normalized by local-friction velocity. For the symbols, see table 1. (*a*) Longitudinal velocity fluctuation. (*b*) Normal velocity fluctuation. (*c*) Lateral velocity fluctuation.

core. By adopting the local scale u_L in figure 12, we have established nearly uniform values of the scaled intensities over the range $0{\cdot}65 < y/h < 1{\cdot}35$. The empirical values describing this region are in fact the constants B_4 to B_6 of equations (3.10), since the 'plateau' extends into the core and, indeed, to the outer edge of the other wall layer. It is somewhat surprising that high-stress and low-stress layers merge after the rather different behaviour near the wall (see figure 9).

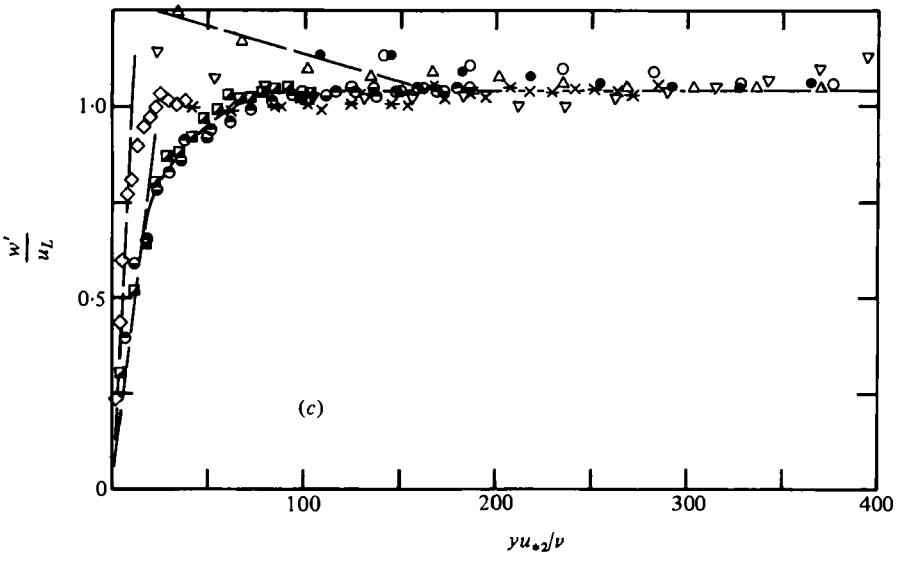

FIGURE 9(c). For legend see p. 301.

Flows	y^+	y/h	Region	μ	u'/u_L	v'/u_L	w'/u_L
Couette-type	<15	—	Viscous	<10	A_4y^+ $A_4 = 0{\cdot}11$ to $0{\cdot}2$	A_5y^{+2} $A_5 = 0{\cdot}0018$ to $0{\cdot}012$	A_6y^+ $A_6 = 0{\cdot}04$ to $0{\cdot}1$
Couette-type	>20	$<1{\cdot}35$	Plateau, core	$<0{\cdot}1$	$B_4 = 1{\cdot}75$	$B_5 = 0{\cdot}8$	$B_6 = 1{\cdot}05$
Couette-type	>50	$<1{\cdot}35$	Plateau, core	$>0{\cdot}1$ <10	$B_4 = 1{\cdot}75$	$B_5 = 0{\cdot}8$	$B_6 = 1{\cdot}05$
Couette-type	>165	$<1{\cdot}35$	Plateau, core	>200	$B_4 = 1{\cdot}75$	$B_5 = 0{\cdot}78$ to $0{\cdot}88$	$B_6 = 1{\cdot}0$ to $1{\cdot}2$

TABLE 4. Similarity results for local-stress scaling (low-stress side). The higher values in the ranges for A_4, A_5, A_6 represent case 9, the lower values represent case 6. The higher values in the ranges for B_5, B_6 represent case 1 ($\gamma = 1$).

4.5. *Core region: Poiseuille-type flows*

Scaling with the local stress, which proved effective for the core of Couette-type flows, is inappropriate here, since the shear stress falls to zero somewhere in the core.

Figure 13 presents the turbulence intensities on the high-stress sides of these flows using the velocity and length scales of equations (3.8). With this scaling most of the data gather near a single line; the resulting empirical constants and limits are given in table 2.

If a like procedure is applied to the low-stress sides of these flows, different formulae are obtained and the scatter is much greater than that of figure 13. Figure 14 gives the turbulence-intensity variations scaled using the effective friction velocity, as

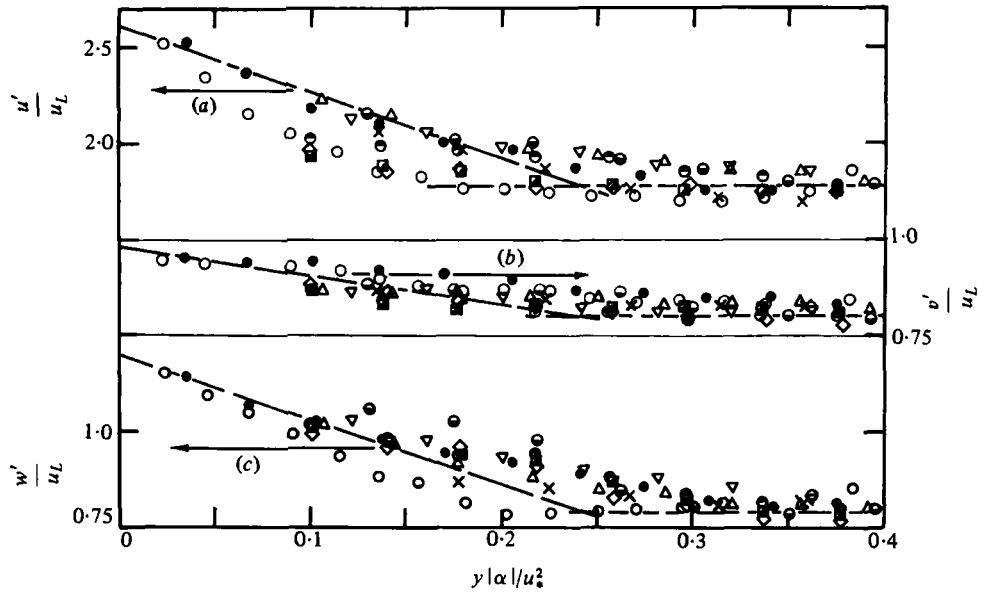

FIGURE 10. Intensity distributions for the high-stress walls of Couette-type flows normalized by local-friction velocity. The symbols × and ○ represent the low-stress and high-stress walls for case 2 respectively; for the other symbols, see table 1. (*a*) Longitudinal velocity fluctuation. (*b*) Normal velocity fluctuation. (*c*) Lateral velocity fluctuation.

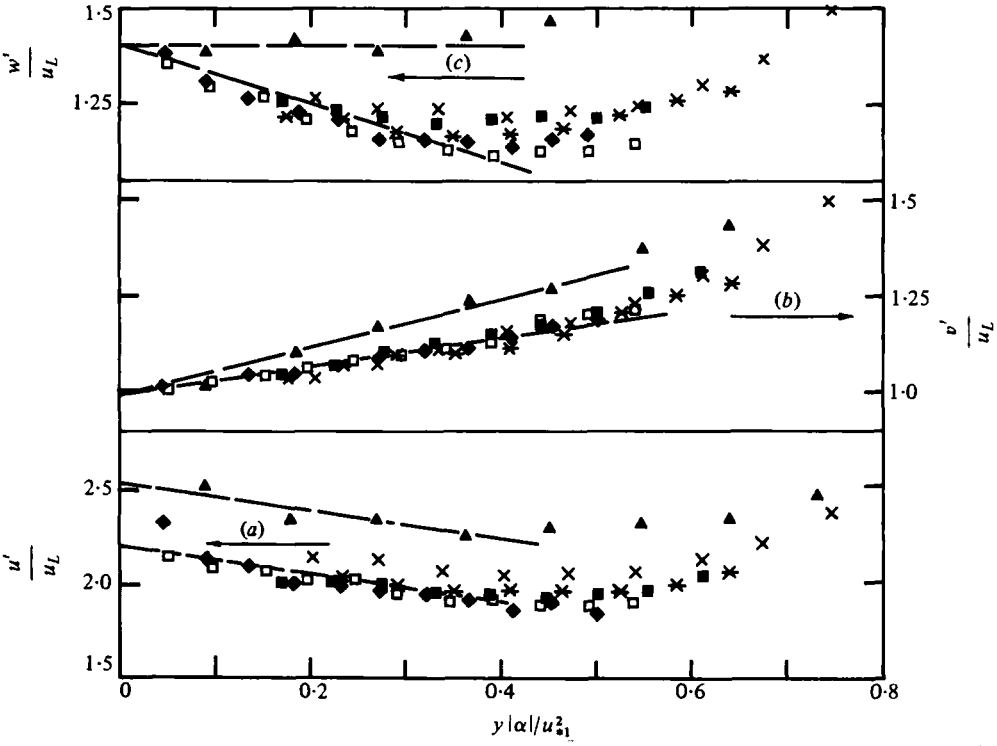

FIGURE 11. Intensity distributions for the high-stress walls of Poiseuille-type flows normalized by local-friction velocity. For the symbols, see table 1. (*a*) Longitudinal velocity fluctuation. (*b*) Normal velocity fluctuation. (*c*) Lateral velocity fluctuation.

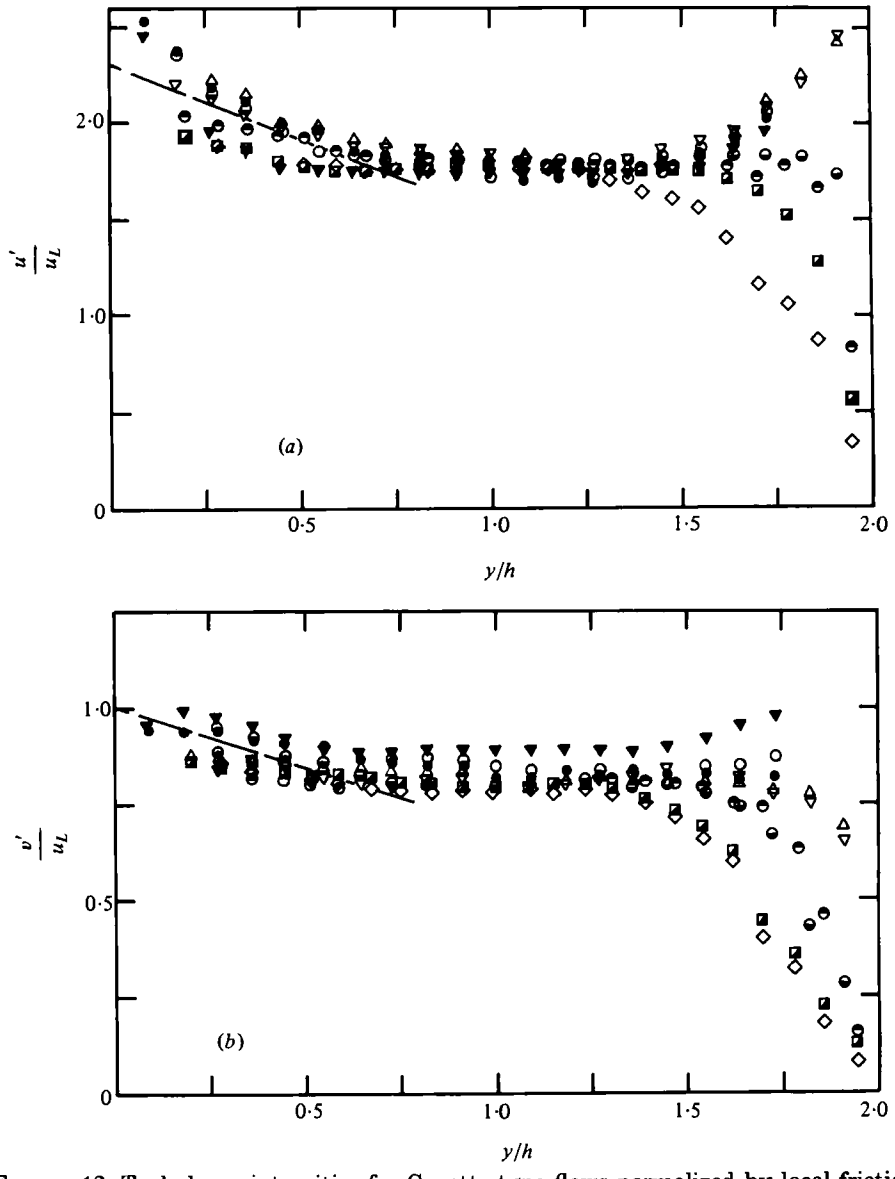

FIGURE 12. Turbulence intensities for Couette-type flows normalized by local-friction velocity (y measured from high-stress wall). For the symbols, see table 1. (*a*) Longitudinal velocity fluctuation. (*b*) Normal velocity fluctuation. (*c*) Lateral velocity fluctuation.

functions of distance measured from the point of maximum velocity. Very approximately, the data are represented by

$$u'/u_e = 1{\cdot}05, \quad v'/u_e = 0{\cdot}55, \quad w'/u_e = 0{\cdot}62. \tag{4.2}$$

4.6. *An overview*

Figure 15 shows the boundaries between the regions in which the several similarity laws have proved to be applicable. We have been able to define reasonably accurate representations of the intensities in the following parts of the flows: (*a*) in the 'linear'

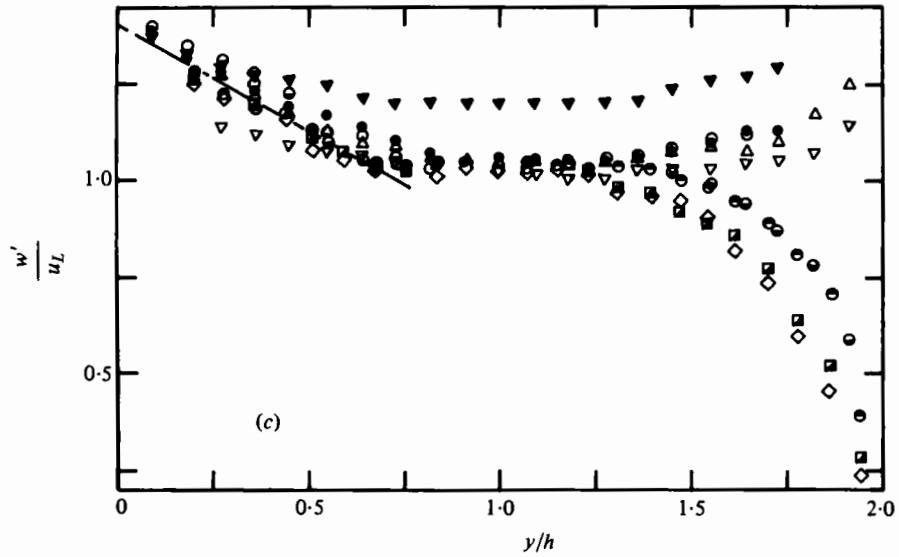

FIGURE 12(c). For legend see p. 304.

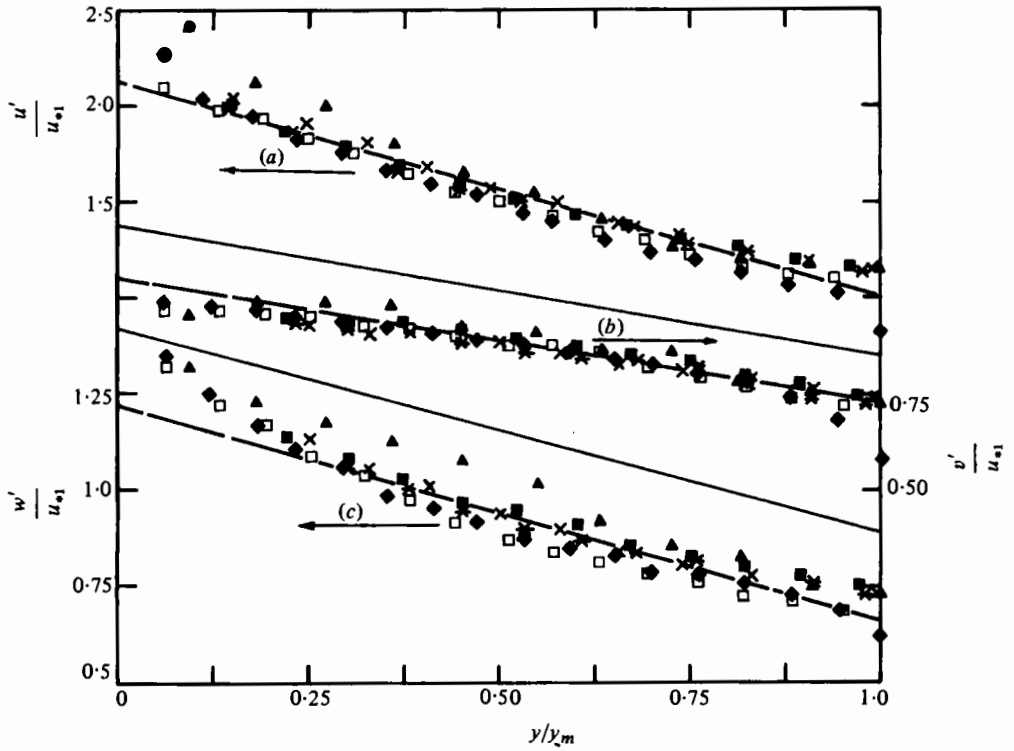

FIGURE 13. Intensity distributions for the high-stress walls of Poiseuille-type flows scaled using wall-friction velocity and length scale for that part of the flow. For the symbols, see table 1. (*a*) Longitudinal velocity fluctuation. (*b*) Normal velocity fluctuation. (*c*) Lateral velocity fluctuation.

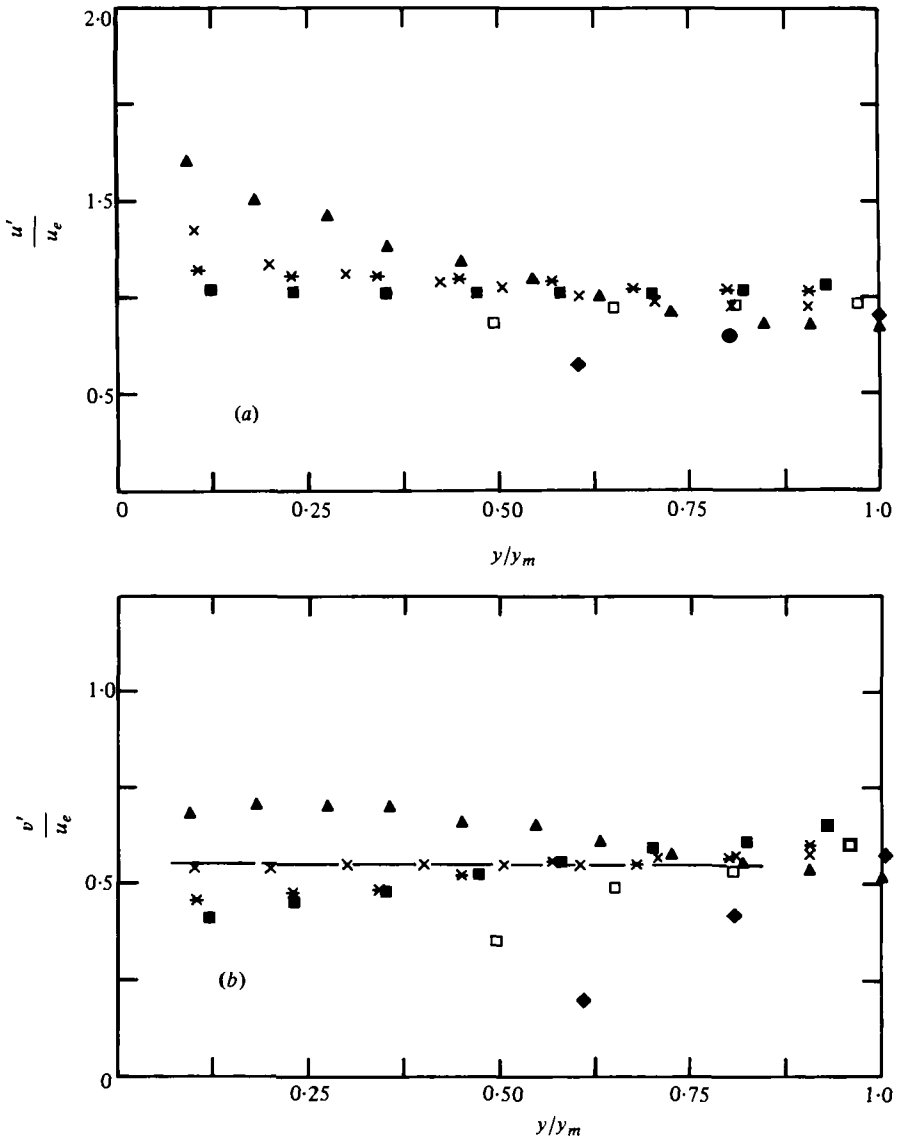

FIGURE 14. Intensity distributions for the low stress walls of Poiseuille-type flows scaled using effective friction velocity (y measured from low-stress wall). For the symbols, see table 1. (a) Longitudinal velocity fluctuation. (b) Normal velocity fluctuation. (c) Lateral velocity fluctuation.

region within L; (b) in the 'plateau' region between V and P^*; (c) in the core region of Couette-type flows between P_1 and P_2; (d) on the high-stress side of Poiseuille-type flows between P_1^* and M.

The regions for which we are not able to provide such convenient representations of the turbulence are: (e) the 'viscous buffer' region between L and V; (f) the 'inviscid buffer' region in Couette-type flows between P^* and P (where we have only approximate results such as equations (4.1); (g) the low-stress side of Poiseuille-type flows between P_2^* and M (where we have only the rough guide of equations (4.2)).

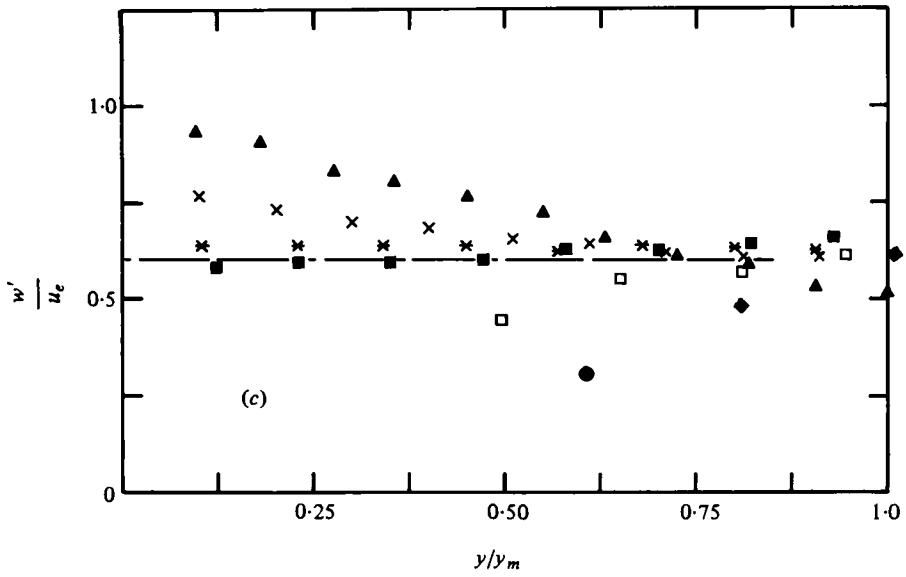

FIGURE 14(c). For legend see p. 306.

Comparison of figure 15 with the corresponding presentation of El Telbany & Reynolds (1980) – figure 12 of that paper, showing regions of applicability for various similarity laws describing the mean velocity – suggests that:

(1) the layer in which viscosity has a significant direct influence is of much the same depth whether defined in terms of mean velocity or in terms of turbulence intensities;

(2) the wall layers defined by a consideration of mean velocities and turbulence intensities are also of roughly the same thickness. However, the simple logarithmic profile for the mean velocity applies over a much more extensive region than does the corresponding intensity plateau derived from wall-stress scaling.

5. Further analysis of the results

5.1. *Other measures of turbulence structure*

To this point we have considered variations in the intensities themselves. We look now at a number of quantities obtained by combining these primitive measures of turbulence structure.

Elsewhere (El Telbany & Reynolds 1981*b*) we have presented these measurements in terms of the quantities (eddy viscosity, mixing length and friction coefficient) commonly used in engineering analysis. The particular case of Couette flow is given more detailed consideration in El Telbany & Reynolds (1981*a*).

The turbulence kinetic energy $\frac{1}{2}q^2 = \frac{1}{2}(u'^2+v'^2+w'^2)$ per unit mass is displayed in figure 16, having been scaled by the effective friction velocity. A noteworthy feature of the results for Couette-type flows is the close grouping of the values for cases in which one wall stress is very small ($\gamma < 0{\cdot}04$, cases 6–9). The corresponding Poiseuille-type flows (case 10 with $\gamma = -0{\cdot}003$ and case 11 with $\gamma = -0{\cdot}075$) display a very

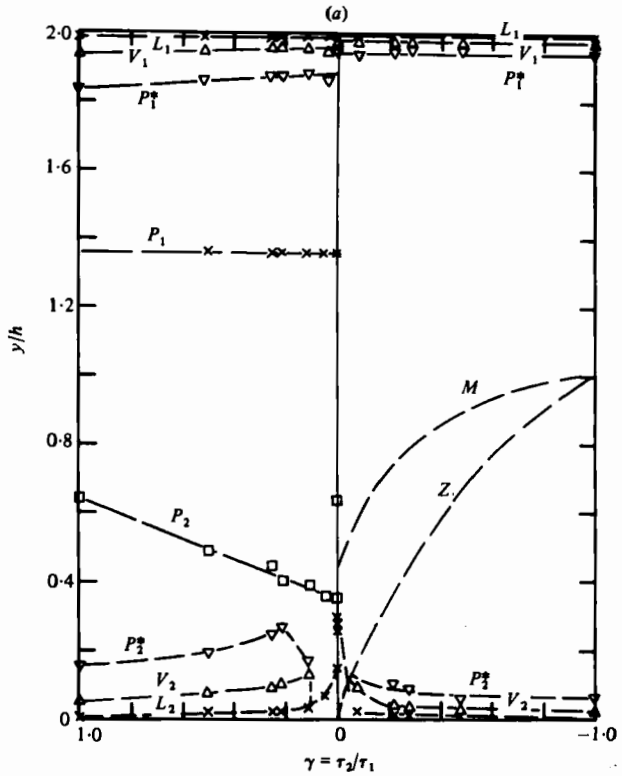

FIGURE 15. Boundaries between regions: L_1, L_2, limits of 'linear' region (as figures 6–8, component normal to wall is in fact quadratic here); V_1, V_2, outer limits of 'viscous buffer' region ($y^+ = 40$); P_1^*, P_2^*, outer limits of 'plateau region' based on wall-stress scaling ($y^+ = 100$ in most cases); P_2, inner limit (for low-stress wall) of 'plateau' region based on local-stress scaling for Couette-type flows (as figure 9); P_1, outer limit (for low-stress wall) of 'plateau' region based on local-stress scaling for Couette-type flows ($y/h = 1{\cdot}35$, figure 12). The lines M and Z denote respectively points of maximum velocity and zero shear stress for Poiseuille-type flows. The co-ordinate y is measured from the low-stress wall. (*a*) Whole of the channel. (*b*) Expansion of region near low-stress wall.

similar trend, but the energy is (according to our measurements) distinctly higher through most of the channel.

The ratio of the turbulent element of the kinematic shear stress to the kinetic energy is plotted in figure 17. For the Poiseuille-type flows of figure 17(*b*), the ratio $-\overline{uv}/\frac{1}{2}q^2$ is reasonably constant near the high-stress wall, then decreases rapidly and reaches zero at the position of zero stress. This pattern is familiar in channel and pipe flows (Laufer 1951, 1954; Comte-Bellot 1965; Hanjalić 1970), and in boundary layers (Klebanoff 1955). In contrast, for the Couette-type flows described by figure 16(*a*) the ratio $-\overline{uv}/\frac{1}{2}q^2$ increases at points progressively further from the wall, then remains nearly constant in the core region, with a considerably higher value (around 0·4) than those characterizing Poiseuille-type flows (0·22–0·32). Again there is a distinct difference between the $\gamma \simeq 0$ cases for Couette-type and Poiseuille-type flows.

A direct proportionality between the shear stress and the kinetic energy is generally

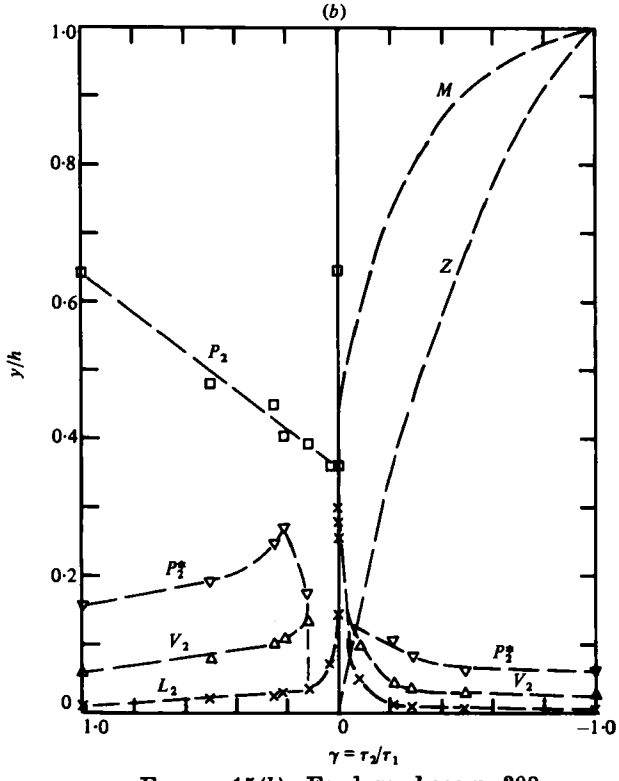

FIGURE 15(*b*). For legend see p. 308.

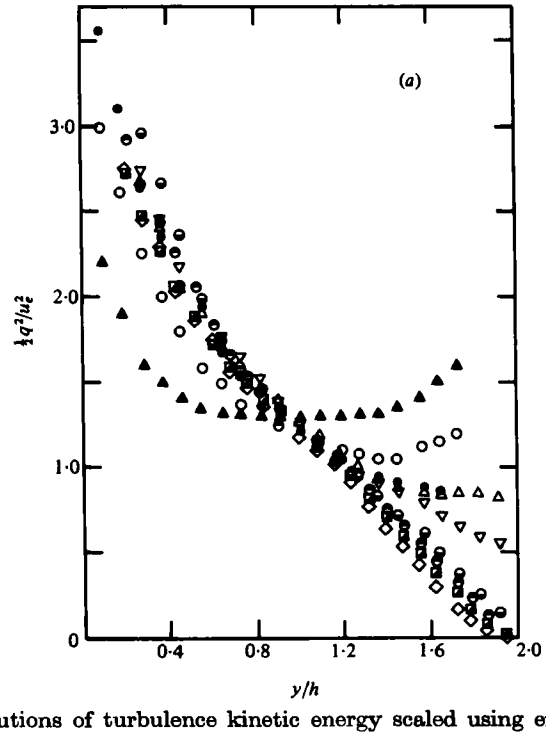

FIGURE 16. Distributions of turbulence kinetic energy scaled using effective friction velocity (y measured from high-stress wall). For the symbols, see table 1. (*a*) Couette-type flows; (*b*) Poiseuille-type flows.

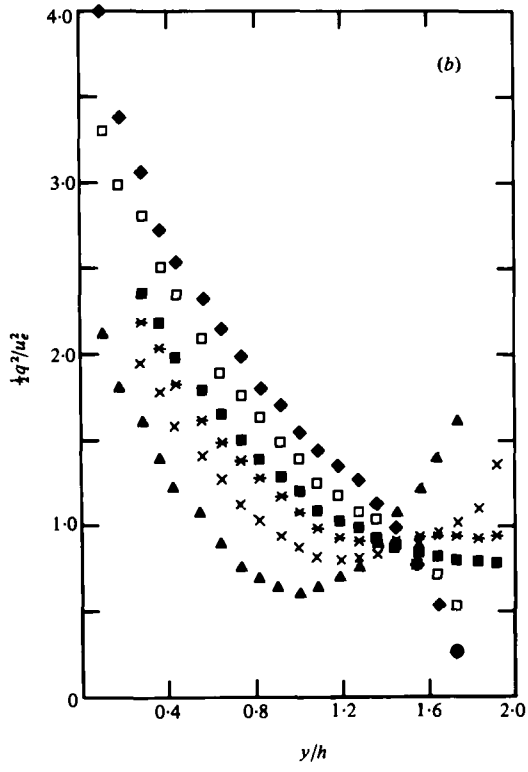

FIGURE 16(*b*). For legend see p. 309.

regarded as a criterion for structural equilibrium of a turbulent flow, characterized by a local balance of energy generation and dissipation (Bradshaw, Ferris & Atwell 1967). Figure 17 indicates that this may be a somewhat superficial view, for it suggests that in Poiseuille-type flows the region of 'structural equilibrium' near the high-stress wall is produced by a rough balance between (*a*) an increase in the length scale at progressively greater distances from the wall, and (*b*) a reduction of the potential ordered activity by the influence of the core, whose nature is in turn determined by the activity near the far wall.

The nearly constant ratios $\overline{uv}/\frac{1}{2}q^2$ characteristic of the flows we have studied are compared with values found by other investigators in table 5. Evidently the constant-pressure boundary layer is most like the limiting Poiseuille-type flow for which $\gamma \simeq 0$. The high values in figure 17(*a*) near $y/h = 1{\cdot}5$ may be a consequence of inaccuracies of measurement. In these flows (cases 7–9) the viscous layer near the low-stress wall is rather deep, and accurate measurement of the small component $\overline{uv}$ becomes difficult. In connection with the observed differences between cases $\gamma \to 0+$ and $\gamma \to 0-$, it is relevant to note that the turbulent element of the shear stress is not eroded so rapidly in the Poiseuille-type limit (compare figure 3(*a*) and (*b*)).

Figure 18(*a*) gives the correlation coefficient $\overline{uv}/u'v'$ for Couette-type flows, while figure 18(*b*) shows this coefficient for Poiseuille-type flows and makes a comparison with Comte-Bellot's (1965) data for pure pressure flow. For the latter case it has often been found that the correlation coefficient is virtually constant and equal to about

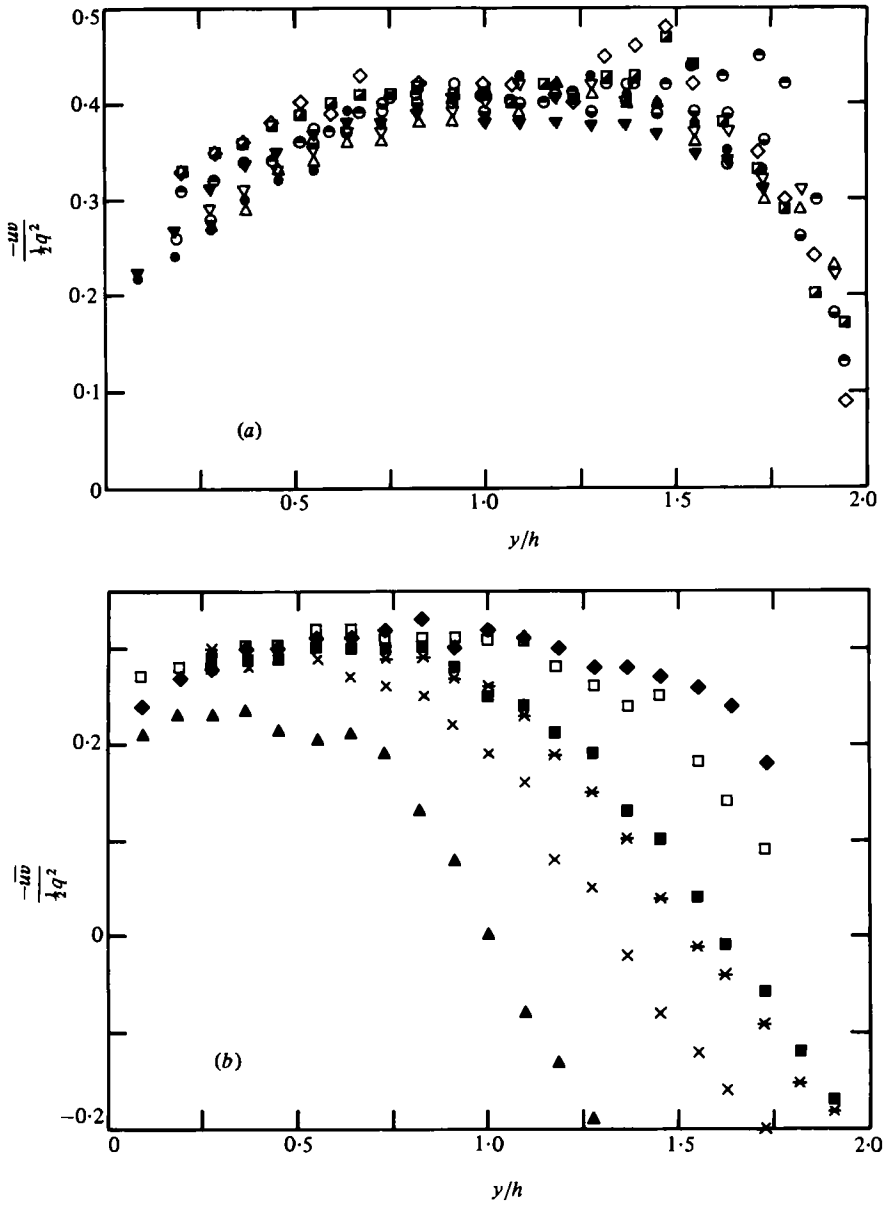

FIGURE 17. Distributions of ratio of turbulent shear stress to kinetic energy (y measured from high-stress wall). For the symbols, see table 1. (*a*) Couette-type flows; (*b*) Poiseuille-type flows.

0·38 over a considerable region near the wall. In figure 18(*b*) this is found to be so once again, and the values are throughout in good agreement with Comte-Bellot's. For the other Poiseuille-type flows, the nearly constant value of the correlation coefficient is rather higher, about 0·45, over a more extensive region extending away from the high-stress wall. (This is closely consistent with the value obtained by Hanjalić (1970), namely $-\overline{uv}/u'v' = 0{\cdot}42$ for $\gamma = -0{\cdot}25$.) As the stress ratio γ decreases, this region extends across the greater part of the channel. Figure 18(*a*) shows that in the present experiments on Couette-type flows the correlation coefficient

Author	Flow type	$-\overline{uv}/\frac{1}{2}q^2$
Laufer (1954)	Smooth-walled pipe flow	0·28
Klebanoff (1955)	Constant-pressure boundary layer	0·32
Comte-Bellot (1965)	Smooth-walled channel ($\gamma = -1$)	0·23
Hanjalić (1970)	Rough-walled channel ($\gamma = -0{\cdot}25$)	0·26
Present	Smooth-walled channel ($\gamma = -1$)	0·23
Present	Smooth-walled channel ($\gamma = -0{\cdot}485$ to $-0{\cdot}0028$)	0·28 to 0·32
Present	Smooth-walled channel ($\gamma > 0$)	0·38 to 0·42

TABLE 5. Comparison of the nearly uniform value of $uv/\frac{1}{2}q^2$.

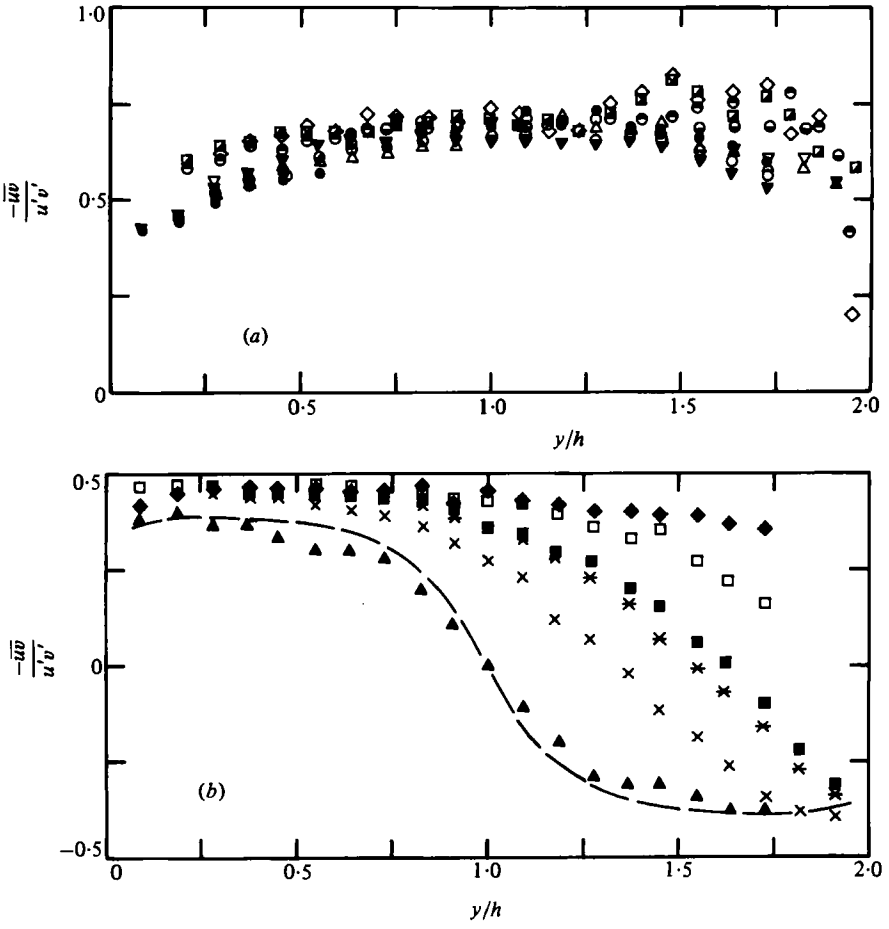

FIGURE 18. Variations of shear correlation coefficient (y measured from high-stress wall). For the symbols, see table 1. (*a*) Couette-type flows; (*b*) Poiseuille-type flows; – – –, Comte-Bellot (1965), $Re = 57\,000$.

rises from a value around 0·4 near the high-stress wall, to a value around 0·7 pertaining throughout the core region. Again cases 7–9 display high values near $y/h \simeq 1{\cdot}5$, probably attributable to the difficulties of measuring the component $\overline{uv}$ in the viscous region near the low-stress wall. Comparison of figure 18(*a*) and (*b*) again indicates that there is a clear difference in the structure of the turbulence (save very near the

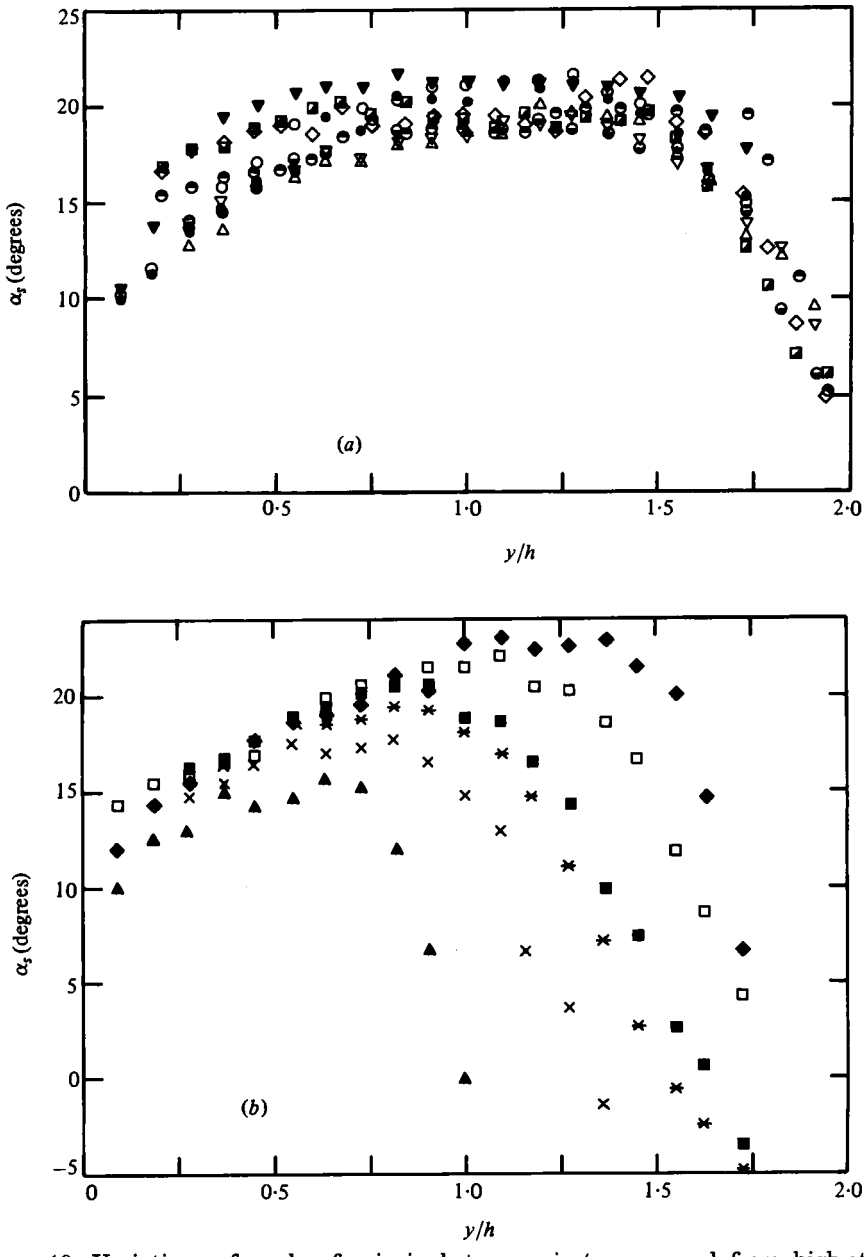

FIGURE 19. Variations of angle of principal-stress axis (y measured from high-stress wall). For the symbols, see table 1. (*a*) Couette-type flows; (*b*) Poiseuille-type flows.

high-stress wall) for cases 9 and 10, the limiting Couette-type and Poiseuille-type flows.

Figure 19 gives the orientation of the principal stress axes. One of the principal directions α_s is shown, calculated from the expression

$$\alpha_s = \tfrac{1}{2}\tan^{-1}\left[\frac{2\overline{uv}}{u'^2 - v'^2}\right].$$

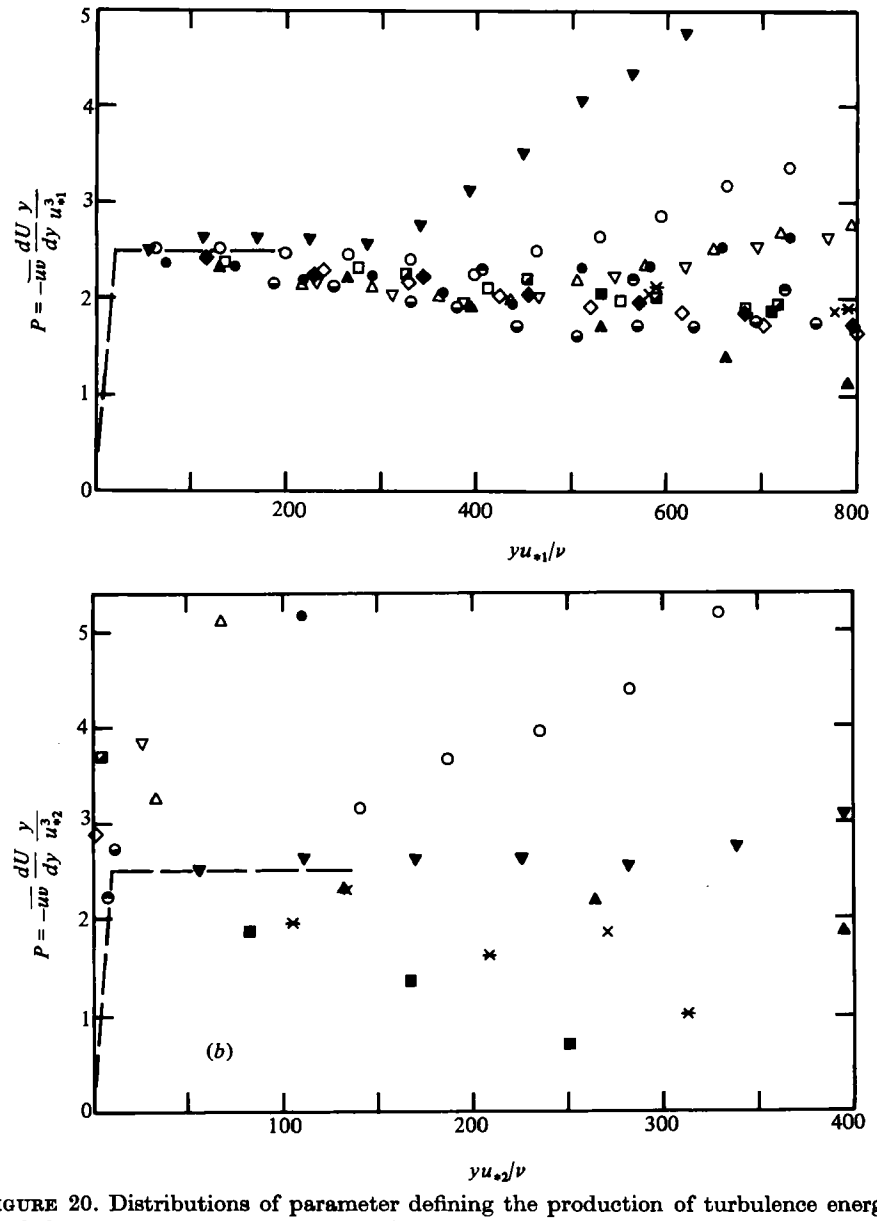

FIGURE 20. Distributions of parameter defining the production of turbulence energy. For the symbols, see table 1. (*a*) y measured from the high stress wall. (*b*) y measured from the low-stress wall.

The variations in this angle are much alike for the whole family of Couette-type flows, and the Poiseuille-type flows also adopt this pattern through about one-half of the channel. In this respect at least the limiting cases for which $\gamma \simeq 0$ behave in a very similar manner.

5.2. *Production of turbulence*

Figure 20 displays variations of the production of turbulence energy, $-\overline{uv}dU/dy$; the two parts of the figure relate, respectively, to high-stress and low-stress walls.

μ	Mean velocity	Turbulence intensities	Turbulence production
1000	Standard constant-stress logarithmic and viscous regions	Standard plateau and viscous regions	$P \simeq 1/K$ for $20 < y^+ < 100$
200	Viscous region unchanged. Logarithmic law for $y^+ < 200$	Plateau and viscous regions intact	
50	Viscous layer occupies a significant fraction of the wall layer; still linear near wall. Logarithmic layer reduced to $y^+ \simeq 150$	No change in viscous region $y^+ < 15$. Plateau almost completely eroded	
10	Viscous layer occupies nearly 20% of the channel; still linear near wall. Logarithmic region nearly vanished	Intensities above constant-stress values even in viscous layer	No region of P = constant
0·3	Viscous layer departs from constant-stress pattern	Intensities generally much higher than constant-stress model	

TABLE 6. Stages in the breakdown of the constant-stress wall layer.

The distance from the wall and the wall friction velocity u_* have been chosen as length and velocity scales.

Figure 20(*a*) shows that for high-stress walls the dimensionless production parameter

$$P = -\frac{\overline{uv}}{u_*^2}\frac{y}{u_*}\frac{dU}{dy} = K^{-1} \simeq 2{\cdot}5$$

for $y_+ < 100$, where K is von Kármán's constant. Indeed, P lies in the range 2·6–2·1 within the more extensive region $y^+ < 300$; this region may then be thought of as the 'standard' constant-stress wall layer.

In figure 20(*b*) we see that the constant-stress layer does not extend even to $y^+ = 100$ on the low-stress sides of the flows labelled in table 1 as cases 2 and 13, for which $\mu = 500$ and 1000 and $|\gamma| = 0{\cdot}3$–$0{\cdot}5$. Moreover, for cases 3 and 12 ($\mu \simeq 300$ and $|\gamma| \simeq 0{\cdot}2$) there is no region in which the values of P characteristic of the constant-stress layer is established.

We conclude then that the distribution of turbulence production near a wall is profoundly influenced by the stress gradient within the wall layer.

5.3. *Erosion of the constant-stress layer*

Both in the mean-velocity measurements of El Telbany & Reynolds (1980) and in the turbulence measurements presented here, there is evidence of a progressive departure of the wall layer from the constant-stress pattern, as the role of the stress gradient becomes more important. The 'standard' constant-stress layer which exists when the parameter $\mu = u_*^3/(|\alpha|\nu) > 1500$ has the following features:

(1) logarithmic variation of mean velocity for $y^+ < 300$;

(2) nearly constant value of the production parameter P for $y^+ < 300$;

(3) a plateau in turbulence intensities (see table 2) for $40 < y^+ < 100$;

(4) a linear variation in mean velocity for $y^+ < 7$; and

(5) simple variations in the intensities for $y^+ < 15$.

The progressive erasure of this pattern as the parameter μ decreases is indicated in table 6. We note that the turbulence structure responds to the encroachment of the stress gradient sooner than does the mean velocity distribution, and that the pattern of turbulence production begins to change before the intensities. This observation brings into question the kind of argument which develops the logarithmic velocity profile by considering a local balance between turbulence production and dissipation.

The picture of the breakdown of the constant-stress layer developed here will relate, in a general way, to the phenomenon of 'relaminarization' in a boundary layer developing in an adverse pressure gradient.

It will be recognized that these attempts to define the changes in the wall layer are based on information about a rather small number of flows; a definitive description would require the study of further layers with very small wall stress. There are indications that the structure of the flow is significantly different for $\gamma < 0$ from that for $\gamma > 0$, but here too the evidence now available is hardly sufficient to justify a more conclusive statement.

6. Conclusions

Many features of the distributions of turbulence intensities in these flows can be explained, or at least presented compactly, using similarity arguments. In particular, 'plateau' regions can be distinguished, using both wall-stress and local-stress scaling, where the intensities are sensibly constant. However, outside the plateau defined by wall-stress scaling there is a region for which it has not been possible to determine an appropriate length scale. That is to say, in this region the influence of the two walls makes itself felt in a complex way and not through the stress gradient alone.

It has been possible to develop simple similarity laws for the high-stress side of Poiseuille-type flows, but no very satisfactory description has been evolved for the low-stress side (save very near the wall, where simple wall-stress scaling is appropriate). Even for those parts of the flows for which we have been relatively unsuccessful in correlating the several sets of measurements it is possible to set down approximate formulae which should be sufficiently realistic for many purposes.

We have been able to sketch out the progressive destruction of the standard constant-stress layer as the role of the stress gradient grows in importance. Standard features of the turbulence vanish before the mean-velocity distribution departs from the constant-stress, logarithmic pattern. Somewhat surprisingly, the turbulence production is the aspect of the flow which is most sensitive to the stress gradient.

There is evidence that the nature of a flow where one wall stress is much smaller than the other is significantly dependent on the sign of the smaller stress through much of the channel, even when that stress is very small indeed. At several points in the preceding discussion we have drawn attention to an apparent discontinuity in the results obtained when the stress at one wall is very small: the measured values were seen to depend critically upon the sign of the nearly vanishing stress at the low-stress wall. In figures 16 and 17 the shift between the turbulence energy distributions for cases 9 and 10 is modest, say 20%, at most. This reflects the measurements of the intensity u' (see figures 4*a* and 5*a*), which makes the dominant contribution to the

turbulence energy. It is in figure 18, which shows the correlation coefficient, that the difference between cases 9 and 10 is most marked, sometimes amounting to 40%. This is so because the normal component v' plays a more significant role; referring to figures 4(*b*) and 5(*b*) we see that the measurements of this quantity are significantly different for cases 9 and 10. Finally, in figure 19 the results for the cases in which $\gamma \simeq 0$ are not too dissimilar, again because the normal component v' does not strongly affect the principal-stress direction.

Summarizing, the measured values of the streamwise and lateral intensities, u' and w', are not significantly different for the two limiting cases of $\gamma \to 0+$ and $\gamma \to 0-$. However, the values of the third component v' do differ, and in consequence so do quantities which depend strongly on v'. We conclude that the sign of the vorticity generated at the low-stress wall has a critical influence on the structure of the turbulence through a large part of the channel, even when the smaller stress is a very small fraction of the dominant stress at the other wall. In the measurements we have made the change in structure has its most obvious effect on the normal component of the turbulent velocity fluctuation.

The apparatus used in these experiments was in large measure designed and developed by Dr M. Farrashkhalvet and Mr M. Kalirai, formerly students of Brunel University. The first author, who is seconded from the Faculty of Engineering, Helwan University, Elmataria, Cairo, has also to acknowledge with thanks the financial assistance of the Egyptian Education Bureau during this investigation.

REFERENCES

Acrivlellis, M. 1977 Hot-wire measurements in flows of low and high turbulence intensity. *DISA Information*, no. 22.

Alcaraz, E., Charnay, G. & Mathieu, J. 1975 Turbulent energy balance in a two-dimensional wall jet developing over a convex surface. *C.R. Acad. Sci. Paris* **280**, 613–616.

Badri Narayanan, M. A. & Ramjee, V. 1969 On the criteria for reverse transition in a two-dimensional boundary-layer flow. *J. Fluid Mech.* **35**, 225–241.

Bradshaw, P. 1969 A note on reverse transition. *J. Fluid Mech.* **35**, 387–390.

Bradshaw, P., Ferris, D. H. & Atwell, H. P. 1967 Calculation of boundary-layer development using the turbulent energy equation. *J. Fluid Mech.* **28**, 593.

Champagne, F. H. & Sleicher, C. A. 1967 Turbulence measurements with inclined hot-wires. II. Hot-wire response equations. *J. Fluid Mech.* **28**, 177–182.

Champagne, F. H., Sleicher, C. A. & Wehrmann, O. H. 1967 Turbulence measurements with inclined hot-wires. I. Heat transfer measurements with inclined hot-wires. *J. Fluid Mech.* **28**, 153–175.

Comte-Bellot, G. 1965 Ecoulement turbulent entre deux parois parallèles. *Publications Scientifiques et Techniques du Ministère de l'air*, no. 419.

El Telbany, M. M. M. & Reynolds, A. J. 1980 Velocity distributions in plane turbulent channel flows. *J. Fluid Mech.* **100**, 1–29.

El Telbany, M. M. M. & Reynolds, A. J. 1981*a* The structure of plane Couette flow. *Trans. A.S.M.E.* I, *J. Fluids Engng* (submitted).

El Telbany, M. M. M. & Reynolds, A. J. 1981*b* The empirical description of turbulent channel flows. *Int. J. Heat Mass Transfer* (in the press).

Hanjalić, K. 1970 Two-dimensional asymmetric turbulent flow in ducts. Ph.D. thesis, University of London.

Hanjalić, K. & Launder, B. E. 1972 Fully developed asymmetric flow in a plane channel. *J. Fluid Mech.* **51**, 301–335.

HATZIAVRAMIDIS, D. T. & HANRATTY, T. J. 1979 The representation of the viscous wall region by a regular eddy pattern. *J. Fluid Mech.* **95**, 655–679.

HINZE, J. O. 1975 *Turbulence.* New York: McGraw-Hill.

HUSSAIN, A. K. M. F. & REYNOLDS, W. C. 1975 Measurements in fully developed turbulent channel flow. *Trans. A.S.M.E.* I, *J. Fluid Engng* **97**, 568–578.

KANEVCE, G. & OKA, S. 1973 Correcting hot wire readings for influence of fluid temperature variations. *DISA Information*, no. 15.

KLEBANOFF, P. S. 1955 Characteristic of turbulence in a boundary layer with zero pressure gradient. *N.A.C.A. Tech. Note*, 1247.

LAUFER, J. 1951 Investigation of turbulent flow in a two-dimensional channel. *N.A.C.A. Rep.* 1053.

LAUFER, J. 1954 The structure of turbulence in fully developed pipe flow. *N.A.C.A. Rep.* 1174.

LAUNDER, B. E. & STINCHCOMBE, H. S. 1967 Non-normal similar turbulent boundary layers. *Mech. Engng Dept. Imperial College, Rep.* TWF/TN/21.

LAWN, C. J. 1969 Turbulence measurements with hot wires at B.N.L. *CEGB, Research and Development Dept., Rep.* RD/B/M1277.

MORRISON, W. R. B. & KRONAUER, R. E. 1969 Structural similarity for fully developed turbulence in smooth tubes. *J. Fluid Mech.* **39**, 117–141.

PATEL, V. C. & HEAD, M. R. 1968 Reversion of turbulent to laminar flow. *J. Fluid Mech.* **34**, 371–392.

PERRY, A. E. & ABELL, C. J. 1977 Asymptotic similarity of turbulence structures in smooth and rough-walled pipes. *J. Fluid Mech.* **79**, 785–799.

ROBERTSON, J. M. & JOHNSON, H. F. 1970 Turbulence structure in plane Couette flow. *J. Engng Mech., A.S.C.E.* **96**, 1171–1182.

SPETTEL, F., MATHIEU, J. & BRISON, J. F. 1972 Tensions de Reynolds et production d'énergie cinétique turbulente dans les jets pariéteux sur parois planes et concaves. *J. Méc.* **11**, 403–425.

TAILLAND, A. & MATHIEU, J. 1967 Jet pariétal. *J. Méc.* **6**, 103–131.

TOWNSEND, A. A. 1961 Equilibrium layers and wall turbulence. *J. Fluid Mech.* **11**, 97–120.

TOWNSEND, A. A. 1976 *The Structure of Turbulent Shear Flow*, 2nd edn, pp. 150–158. Cambridge University Press.

WEBSTER, C. A. 1962 A note on the sensitivity to yaw of a hot wire anemometer. *J. Fluid Mech.* **13**, 307–312.